and Barbera, P.: Sulfhydryl groups and peroxidase-like activity of albumin as scavenger of organic peroxides. *Pharmacol. Res. Commun.*, **20**: 545-552 (1988).
13) Harada, D., Naito, S., Kawauchi, Y., Ishikawa, K., Koshitani, O., Hiraoka, I. and Otagiri, M.: Determination of reduced, protein-unbound, and total concentrations of N-acetyl-L-cysteine and L-cysteine in rat plasma by post-column ligand substitution high-performance liquid chromatography. *Anal. Biochem.*, **290**: 251-259 (2001).

Available online at www.sciencedirect.com
SCIENCE DIRECT
Biochimica et Biophysica Acta 1675 (2004) 21–31
BIOCHIMICA ET BIOPHYSICA ACTA
BBA
http://www.elsevier.com/locate/bba

Physicochemical characterization of cross-linked human serum albumin dimer and its synthetic heme hybrid as an oxygen carrier

Teruyuki Komatsu[a], Yukiko Oguro[a], Yuji Teramura[a], Shinji Takeoka[a], Junpei Okai[b], Makoto Anraku[b], Masaki Otagiri[b], Eishun Tsuchida[a,*]

[a]*Advanced Research Institute for Science and Engineering, Waseda University, 3-4-1 Okubo, Shinjuku-ku, Tokyo 169-8555, Japan*
[b]*Department of Pharmaceutics, Faculty of Pharmaceutical Sciences, Kumamoto University, 5-1 Oe-honmachi, Kumamoto 862-0973, Japan*

Received 13 May 2004; received in revised form 9 August 2004; accepted 10 August 2004
Available online 11 September 2004

Abstract

The recombinant human serum albumin (rHSA) dimer, which was cross-linked by a thiol group of Cys-34 with 1,6-bis(maleimido)hexane, has been physicochemically characterized. Reduction of the inert mixed-disulfide of Cys-34 beforehand improved the efficiency of the cross-linking reaction. The purified dimer showed a double mass and absorption coefficient, but unaltered molar ellipticity, isoelectric point (p*I*: 4.8) and denaturing temperature (65 °C). The concentration dependence of the colloid osmotic pressure (COP) demonstrated that the 8.5 g dL^{-1} dimer solution has the same COP with the physiological 5 g dL^{-1} rHSA. The antigenic epitopes of the albumin units are preserved after bridging the Cys-34, and the circulation lifetime of the ^{125}I-labeled variant in rat was 18 h. A total of 16 molecules of the tetrakis{(1-methylcyclohexanamido)phenyl}porphinatoiron(II) derivative (FecycP) is incorporated into the hydrophobic cavities of the HSA dimer, giving an albumin–heme hybrid in dimeric form. It can reversibly bind and release O_2 under physiological conditions (37 °C, pH 7.3) like hemoglobin or myoglobin. Magnetic circular dichroism (CD) revealed the formation of an O_2–adduct complex and laser flash photolysis experiments showed the three-component kinetics of the O_2-recombination reaction. The O_2-binding affinity and the O_2-association and -dissociation rate constants of this synthetic hemoprotein have also been evaluated.

Keywords: Human serum albumin dimer; Cross-linking; Colloid osmotic pressure; Synthetic heme; Albumin–heme dimer; Oxygen carrier

1. Introduction

Human serum albumin (HSA) is the most abundant plasma protein and contains 35 cysteines, of which 17 couples form intramolecular disulfide bonds to fold a single polypeptide as a unique heart-shape structure [1–4]. Only the first thiol residue in the chain, namely Cys-34, does not participate in the S–S bonding and functions as a binding site for the SH-involving ligands (cysteine, glutathione, and captopril), as well as for the various metal ions and nitric oxide [1,5]. Interestingly, two albumin molecules can associate to produce a dimer through an intermolecular disulfide bridge of Cys-34; approximately 5% of HSA is actually in a dimeric form in our bloodstream [6]. Hughes [7] initially prepared the HSA dimer by the addition of bifunctional $HgCl_2$, which causes Cys-34 to connect through mercury. Subsequent oxidation of this mercury dimer by treatment with iodine gave a disulfide-linked HSA [8]. It can also be directly prepared by oxidation of HSA with ferricyanide [9]. However, electron spin resonance measurements of HSA and the latest crystal structural analysis of the recombinant HSA (rHSA) revealed that Cys-34 locates in a hydrophobic crevice at a depth of 9.5 Å from the surface [2–4,10]. This implies that the intermolecular Cys-34 disulfide bridging might lead to flattening of the pocket. We have linked two rHSA molecules with a flexible bola-shape spacer, 1,6-bis(maleimido)hexane (BMH), which is long (16 Å) enough to connect the Cys-34 residues, to produce a new type of rHSA dimer (Fig. 1) [11].

* Corresponding author. Tel.: +81 3 5286 3120; fax: +81 3 3205 4740.
E-mail address: eishun@waseda.jp (E. Tsuchida).

0304-4165/$ - see front matter © 2004 Elsevier B.V. All rights reserved.
doi:10.1016/j.bbagen.2004.08.010

(A)

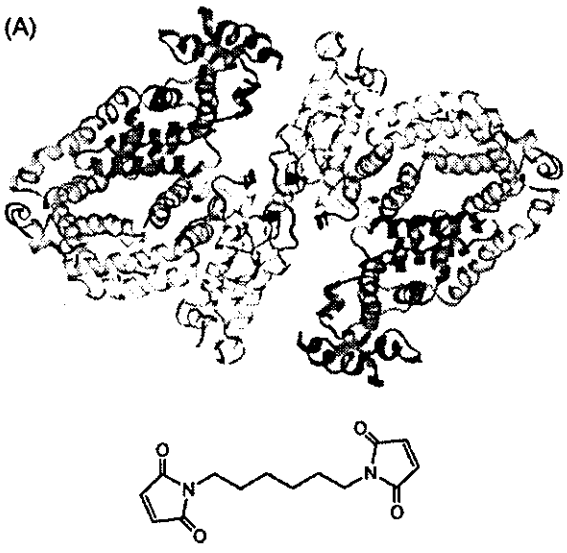

1,6-Bis(maleimido)hexane (BMH)

(B)

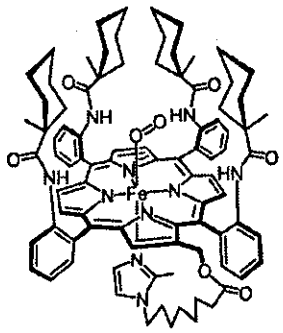

FecycP

Fig. 1. (A) Simulated structure of rHSA dimer cross-linked by Cys-34 with 1,6-bis(maleimido)hexane (BMH). The domains I, II, and III of each rHSA unit are colored white, yellow, and pink, respectively. The cross-linking agent (BMH) is shown in a space-filling representation and colored by atom type (carbon: green, nitrogen: blue, oxygen: red). The figure was made with insight II (Molecular Simulations) on the basis of the 1c78 available at the Brookhaven PDB. (B) Formula of synthetic heme, FecycP.

On the other hand, a maximum of eight molecules of synthetic heme with a covalently bound proximal base is incorporated into the hydrophobic cavities of rHSA, giving an albumin–heme hybrid, which can reversibly bind and release O_2 under physiological conditions (pH 7.3, 37 °C) like hemoglobin (Hb) or myoglobin (Mb) [12]. We have shown that this O_2-carrying plasma protein acts as a red blood cell (RBC) substitute in vitro and in vivo [13]. The only fault of this system is its relatively low heme concentration, which reflects the O_2 solubility in the medium. For instance, the albumin–heme solution with a physiological HSA concentration (≈0.75 mM) involves 6 mM of heme, which corresponds to only 65% of the amount in human blood ([heme]=9.2 mM). A highly condensed solution can dissolve more heme, however, the colloid osmotic pressure (COP) increases in proportion to the albumin concentration. We have found that a total of 16 molecules of 2-[8-{*N*-(2-methylimidazolyl)}octanoyloxymethyl]-5,10,15,20-tetrakis{α,α,α,α-*o*-(pivalamido)phenyl}porphinatoiron(II) (FepivP) was incorporated into the BMH-bridged HSA dimer, and this solution with 0.75 mM HSA includes 12 mM of heme [11]. The tertiary structures of the two protein-units might be intact after the cross-linking, and the ligand-binding capacity of the dimer became twofold in excess relative to that of the monomer. Consequently, the saline solution of the albumin–heme dimer can transport a large volume of O_2 in comparison to the human blood while maintaining its COP on a physiological level. A long persistence in circulation due to the large molecular size is also expected. In this paper, we report the efficient synthesis, physicochemical characterization, and preliminary pharmacokinetics of the BMH-bridged rHSA dimer. Furthermore, the O_2-binding properties of the albumin-heme dimer incorporating the FepivP analogue, 2-[8-{*N*-(2-methylimidazolyl)}octanoyloxymethyl]-5,10,15,20-tetrakis{α,α,α,α-*o*-(1-methylcyclohexanamido)phenyl}porphinatoiron(II) (FecycP, Fig. 1), are evaluated by magnetic circular dichroism and laser flash photolysis.

2. Material and methods

2.1. Materials

An rHSA (Albrec®, 25 wt.%) was provided from the NIPRO (Osaka). Ethanol, dithiothreitol (DTT), 2,2′-dithiopyridine, and warfarin (all high-purity grades) were purchased from Kanto Chemical, (Tokyo) and used without further purification. 1,6-Bis(maleimido)hexane was purchased from Pierce Biotechnology (Rockford, USA). Diazepam was purchased from Wako Pure Chemical Ind., (Tokyo). 2-[8-{*N*-(2-Methylimidazolyl)}octanoyloxymethyl]-5,10,15,20-tetrakis{α,α,α,α-*o*-(1-methylcyclohexanamido)phenyl}porphinatoiron(II) (FecycP) was prepared according to our previously reported procedure [14].

2.2. Synthesis of rHSA dimer

Aqueous DTT (1.0 M, 0.24 mL) was added to the phosphate buffer solution (pH 7.0, 10 mM) of rHSA (0.75 mM, 80 mL) under nitrogen, and the solution was quickly mixed by a vortex mixer, followed by an incubation for 30 min at room temperature. The obtained rHSA in reduced form was washed with a total of 880-mL phosphate buffer (pH 7.0, 2.25 mM) using an ADVANTEC UHP-76K ultrafiltration system with a Q0500 076E membrane (cutoff Mw 50 kDa) and finally condensed to 26.7 mL ([rHSA]=2.25 mM). The mercapto-ratio of the Cys-34

was confirmed by the reaction with 2,2′-ditiopyridine (2,2′-DTP), which immediately coupled with the free thiol group to give 2-thiopyridinone (2-TP) with an absorption at 343 nm [molar absorption coefficient (ε_{343}): 8.1×10^3 M^{-1} cm^{-1}]. Quantitative assay of the produced 2-TP showed that the mercapto-ratio of Cys-34 was 100%. Ethanolic BMH (6.38 mM, 4.76 mL) divided into three portions was then slowly added dropwise into the rHSA solution within 1 h under an N_2 atmosphere, and gently stirred overnight at room temperature. The reaction kinetics was observed by the HPLC measurements. The HPLC system consisted of a Shimadzu LC-8A pump and a Shimadzu SPD-10A UV detector. A Shodex Protein KW-803 column was used and the mobile phase was phosphate buffered saline (PBS, pH 7.4) at 25 °C (1.0 mL min^{-1}). The dimer was purified by gel column chromatography with Sephacryl S-200 HR (Pharmacia, 5 cmϕ×40 cm) and PBS (pH 7.4) as the eluant (5.0 mL min^{-1}). These separations were performed using a BIO-RAD EGP Combo Rec system. The elution was monitored by absorption at 280 nm. The purity of the dimer was measured by the HPLC technique described above. The albumin concentrations were assayed by general bromcresol green (BCG) methods using a Wako AlbuminB-Test [15].

2.3. Physicochemical properties

The UV–Vis absorption spectra were recorded on a JASCO V-570 spectrophotometer. The measurements were normally carried out at 25 °C. Circular dichroism (CD) spectra were obtained using a JASCO J-725 spectropolarimeter. The rHSA samples' concentration was 2 μM in PBS, and quartz cuvettes with a 1-mm thickness were used for the measurements over the range of 195–250 nm. The matrix associated laser desorption ionization time-of-flight mass spectra (MALDI-TOF MS) were obtained using a Shimadzu AXIMA-CFR Kompact MALDI, which was calibrated by BSA (Sigma A-0281) and HSA (Sigma A-3782). The specimens were prepared by mixing the aqueous sample solution (10 μM, 1 μL) and matrix (10 mg mL^{-1} sinapinic acid in 40% aqueous CH_3CN, 1 μL) on the measuring plate and drying in air. The viscosity and density of the rHSA solutions (PBS, pH 7.4) were obtained using an Anton PAAR DSC 300 capillary viscometer at 37 °C. The isoelectric points and molecular weights were obtained by a Pharmacia Phastsystem using isoelectric focusing (IEF) in Phast Gel IEF 3-9 and Native-PAGE in Phast Gel Gradient 8–25, respectively. The colloid osmotic pressures of the rHSA solutions (PBS, pH 7.4) were measured by a WESCOR 4420 Colloid Osmometer at 25 °C. A membrane filter with a 30-kDa cutoff was used. Differential scanning calorimetry (DSC) was measured on a SEIKO Instruments DCS120 differential scanning calorimeter at the scan rate of 1 °C min^{-1} in the temperature range between 10 and 95 °C. The concentrations of the rHSA samples were 75 μM in PBS (pH 7.4).

2.4. Ligand binding constants

The PBS solution of ligand (warfarin or diazepam, 20 μM, 2 mL) was mixed with the rHSA sample in PBS (20 μM, 2 mL), and the unbound ligand fractions were separated by centrifugation (2000 rpm, 25 °C, 20 min) using a Millipore Centriplus YM-50. Adsorption of the ligand molecules onto the filtration membranes was negligible. The unbound ligand concentrations were determined by UV–Vis spectroscopic measurements.

2.5. Compatibility with blood components in vitro

Fresh whole blood was obtained from Wistar rats (300 g, male, Saitama Experimental Animals Supply, Japan) and stored in heparinized glass tubes. The rHSA samples (PBS, pH 7.4) were then slowly added to the blood at 50 vol.% concentrations (whole volume 2 mL). After 30 min, 30 μL of the sample was mixed with 100 μL of a Terumo ACD-A solution, which was diluted in advance with pure water by 1:10 (v/v). The blood cell numbers of the obtained samples were counted using a Sysmex KX-21 blood cell counting device. Furthermore, one drop of the incubated sample of the blood with the rHSA dimer was microscopically observed using an Olympus IX50 microscope with an IX70 CCD camera.

2.6. Immunogenicity

The Tris–HCl buffer solutions (TBS, pH 7.4, 50 mM, 50 μL) of the rHSA samples (10 μg mL^{-1}) were injected into a Nunc immunoplate and incubated at 4 °C overnight. The rHSA solutions in the wells were washed with TBS, and 2% skimmed milk was added to avoid the nonspecific binding of the antibody. After washing with TBS including 0.1% Tween 20 (Tween 20–TBS), anti-HSA polyclonal antibody (50 μL per well) was added and incubated for 2 h at 25 °C. The antibody was removed by aspiration, and 50 μL of horseradish peroxidase-labelled rabbit anti-IgG polyclonal antibody diluted 1/5000 by Tween 20–TBS was injected, following an incubation for 1 h at 25 °C. Finally, 100 μL of *o*-phenylenediamine substrate solution (400 mg mL^{-1} in 0.15 M citrate-phosphate buffer (pH 5.0) involving 0.1% H_2O_2) was put into each well. H_2SO_4 (2 M; 50 μL) was then added to stop the reaction. The resulting absorbance in each well was measured at 490 nm using a Japan InterMed Imunomini NJ-2300.

2.7. Circulation lifetime in vivo

The 125-Iodinated rHSA monomer and dimer were prepared by our previously reported procedures, and purified using a Pharmacia Bio-Gel PD-10 column [16]. The recovered ^{125}I-albumin had a specific activity of 2.0×10^7 cpm μg^{-1}, and was diluted by non-labeled albumin before intracardial administration into anesthetized Wistar rats

(200–210 g, male). The kinetics of the albumin clearance from the circulation was monitored by measuring the radioactivity in the plasma phase of blood taken from the lateral tail veins using an Aloka ARC 2000 Autowell Gamma Counter. Acid precipitability of the recovered radioactivity was also measured. The aqueous trichloroacetic acid (TCA, 25%, 0.1 mL) was first added to the plasma (20 μL) diluted with 5 g dL^{-1} rHSA (80 μL), followed by centrifugation (3000 rpm, 10 min). The precipitate was then washed with 12.5% TCA (0.2 mL) and the radioactivity of the pellet was measured. The rats were sacrificed at the end of the experiments by hemorrhage. The radioactivity of the excised organs was also measured as well. The care and handling of the animals were in accordance with NIH guidelines.

2.8. Preparation of albumin–heme dimer

The preparation of rHSA–FecycP dimer was carried out by mixing the EtOH solution of carbonyl-FecycP and an aqueous phosphate buffer solution of rHSA according to our previously reported procedures ([FecycP]/[rHSA]=16:1 (mol/mol)) [13]. The albumin concentrations were assayed by the general BCG methods described above, and the amount of FecycP was determined by the assay of the iron ion concentration using inductively coupled plasma spectrometry (ICP) with a Seiko Instruments SPS 7000A spectrometer.

2.9. Magnetic circular dichroism (MCD)

MCD spectra for the phosphate buffer solution of the rHSA–FecycP dimer (10 μM) under N_2, CO, and O_2 atmospheres were measured using a JASCO J-820 circular dichrometer fitted with a 1.5-T electromagnet. The accumulation times were normally three, and from each data point was subtracted the spectra without an electromagnetic (at 0 T) as the baseline.

2.10. O_2-Binding equilibrium and kinetics

O_2-Binding to FecycP was expressed by Eq. (1).

$$\text{FecycP} + O_2 \underset{k_{off}}{\overset{k_{on}}{\rightleftharpoons}} \text{FecycP}(O_2) \quad (K = k_{on}/k_{off}) \tag{1}$$

The O_2-binding affinity (gaseous pressure at half O_2-binding for heme, $P_{1/2}=1/K$) was determined by spectral changes at various partial pressure of O_2 as in previous reports [12,a,d,14]. The FecycP concentrations of 20 μM were normally used for the UV–Vis absorption spectroscopy. The spectra were recorded within the range of 350–700 nm. The half lifetime of the dioxygenated species of the rHSA–FecycP dimer was determined by the time dependence of the absorption intensity at 549 nm, which is based on the O_2–adduct complex. The association and dissociation rate constants for O_2 (k_{on}, k_{off}) were measured by a competitive rebinding technique using a Unisoku TSP-600 laser flash photolysis apparatus [12,17–19]. The absorption decays accompanying the O_2 association to the rHSA–FecycP dimer obeyed three-component kinetics. We employed triple-exponentials to analyze the absorption decays; $\Delta A(t)$ [12,a,b,],

$$\Delta A(t) = C_1\exp(-k_1 t) + C_2\exp(-k_2 t) + C_3\exp(-k_3 t) \tag{2}$$

where k_1, k_2, k_3 are apparent rate constants for the each reaction. The data were fit to this equation using a Solver in Excel 2003.

3. Results and discussion

3.1. Synthesis of rHSA dimer

In the neutral pH range (5.0–7.0), DTT selectively reduces the mixed-disulfide of Cys-34 in HSA or BSA [20–22]. In fact, the addition of the small molar excess DTT into the rHSA solution (phosphate buffer, pH 7.0, 10 mM) under an N_2 atmosphere led to complete reduction of Cys-34 (mercapto-ratio became 100%). After removing DTT, ethanolic BMH was dropwise added to the reduced rHSA to initiate the cross-linking reaction. The pretreatment with DTT significantly increased the yield of the dimer, and the rHSA concentration of 15 g dL^{-1} gave the highest yield of 45%, which is significantly improved from our previous result (Fig. 2) [11]. Several attempts to facilitate the dimerization

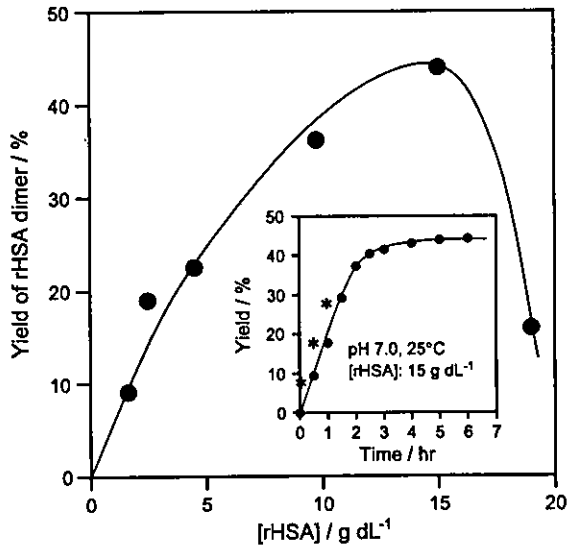

Fig. 2. The relationship between the rHSA concentration and yield of the rHSA dimer. The yields were determined based on the peak area in the HPLC elution curves. Inset shows the time course of the dimerization yield when the rHSA concentration was set at 15 g dL^{-1}. The asterisks indicate the time points when the EtOH solution of BMH was dropwise added. The total EtOH content in the reaction mixture was 15 vol.%.

unfortunately failed: (i) gentle heating (25–50 °C), (ii) changing the co-solvent from EtOH to DMF for dissolving the BMH, and molar ratio [BMH]/[rHSA]: 0.5–1.5, (iii) increasing the concentrations of co-solvents (<30%), and (iv) the further addition of the reactive rHSA monomer.

The HPLC elution curve of the reactant demonstrated only two peaks (rHSA monomer and dimer), which means that the bifunctional BMH was successfully bound to Cys-34 which led to dimer formation and not polymerization (Fig. 3). The yield reached a peak within 4 h (Fig. 2 inset). The addition of EtOH to the mixture (40 vol.%) immediately formed a white precipitate; this is similar to the well-known Cohn's methods [1,23]. However, the precipitate still contained the monomer component. In contrast, separation using gel column chromatography with Sephacryl S-200 HR gave the dimer with 99% purity and 80% recovery. Native-PAGE showed a single band in the molecular weight range of 13 kDa (Fig. 3, above). We could not detect the free thiol in the isolated rHSA dimer (mercapto-ratio: 0%), which is now available in gram quantities. The appearance of the obtained dimer solution (in PBS, 20 g dL^{-1}) did not change over 1 year at room temperature and underwent no aggregation and precipitation.

3.2. Physicochemical properties

The matrix associated laser desorption ionization time-of-flight mass spectroscopy (MALDI-TOF MS) of the BMH-bridged rHSA dimer showed a distinct sharp signal at *m/z* 132,741.3, which is in good agreement with the calculated mass (Mw. 133,179.6); the difference was only 0.3% (Table 1). The magnitudes of its UV–Vis absorption (λ_{max}: 280 nm) significantly increased compared to that of

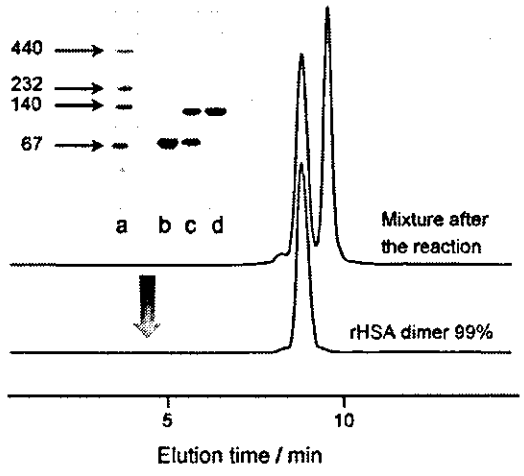

Fig. 3. HPLC elution curves of the rHSA dimer at 25 °C. The upper profile after the reaction indicated that the reactant consists of only the monomer and dimer. After gel column chromatography, the rHSA dimer was isolated with the purity of 99%. The left upper pattern is the native-PAGE electrophoresis of the rHSA dimer. a: markers, b: rHSA, c: mixture after the reaction, d: purified rHSA dimer.

Table 1
Physicochemical properties of rHSA dimer

	rHSA	rHSA dimer
Mw (Da)	66,331[a]	132,741[a]
	66×10^3 [b]	136×10^3 [b]
[calculated value]	66,451	133,180
Cys-34 mercapto ratio (%)	17	0
pI	4.8	4.8
ε_{280} (cm^{-1} M^{-1})	3.4×10^4	6.8×10^4
$[\theta]_{208}$ (deg cm^2 $dmol^{-1}$)	1.9×10^4	1.9×10^4
$[\theta]_{222}$ (deg cm^2 $dmol^{-1}$)	1.8×10^4	1.8×10^4

[a] Determined by MALDI-TOF/MS.
[b] Determined by [C] vs. COP/[C] (Fig. 5, inset).

rHSA with the same molar concentrations (Fig. 4(A)). The concentration of the albumin was carefully assayed by (i) BCG method [15] and (ii) weighing method with the weight of the freeze-dried sample and its molecular weight. While the molar absorption coefficient at 280 nm (ε_{280}: 6.8×10^4 M^{-1} cm^{-1}) became exactly twice the monomer's value (3.4×10^4 M^{-1} cm^{-1}), the CD spectral pattern (λ_{min}: 208, 222 nm) and the molar ellipticities at 208 and 222 nm ($[\theta]_{208}$: 1.9×10^4 deg cm^2 $dmol^{-1}$, $[\theta]_{222}$: 1.8×10^4 deg cm^2 $dmol^{-1}$) were identical to those of the monomer (Fig. 4(B), Table 1) [24,25]. It is appropriate to consider that the α-helix content of the each rHSA unit (67%) was unaltered [1–4]. The isoelectric point of the dimer (*pI*: 4.8) was also the same as that of rHSA. All these observations suggested that the secondary/tertiary structure and surface net charges of the rHSA units in the dimer did not change after the S–S disulfide bridging of Cys-34.

The DSC thermogram of this rHSA dimer showed an exothermic peak at 65 °C, which corresponds to its denaturing temperature (T_d). It has been shown that the T_d of HSA is largely dependent on the content of the

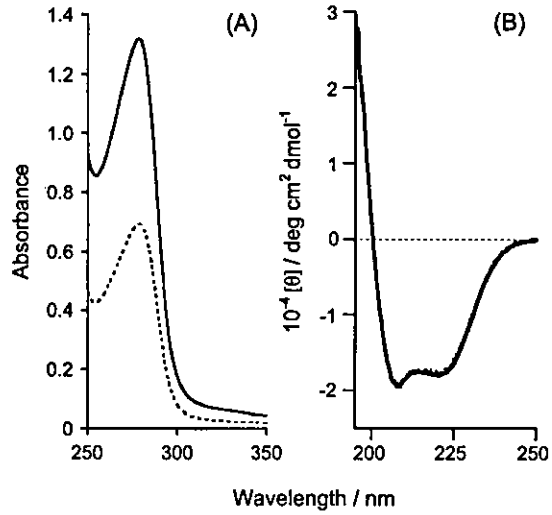

Fig. 4. (A) UV–Vis absorption spectra and (B) CD spectra of rHSA monomer (dotted line) and rHSA dimer (solid line) in PBS solution (pH 7.4) at 25 °C.

incorporated fatty acid, pH, and ionic strength [26,27]. In general, pasteurization for plasma HSA is performed at 60 °C for 10 h to eliminate the contaminations, e.g., hepatitis, HIV, and herpes virus [1]. Sodium caprylate and sodium *N*-acetyl-L-tryptophanate are commonly added to stabilize the albumin structure during the heat treatment [26]. Since the thermogram of the rHSA monomer under our sample conditions (PBS, pH 7.4) showed the T_d at 63 °C, we concluded that the rHSA dimer has the same thermodynamic stability with the monomer. Only the enthalpy change during the denaturation (ΔH) was slightly lower than the twice the monomer's value.

HSA acts as a carrier for many endogenous and exogenous substances in the blood circulation, and has two major specific drug binding sites, namely the warfarin site (Site I) and the indole and benzodiazepine site (Site II) [1,28]. We then determined the binding constants of typical ligands, warfarin (Site I-ligand) and diazepam (Site II-ligand), for the rHSA dimer using the ultracentrifugation method. In contrast to the results of the control experiments with rHSA, the amount of unbound ligand decreased to nearly half. The equilibria are expressed by following equations:

$$D + L \overset{K_1}{\rightleftharpoons} D\text{-}L \quad (3)$$

$$D\text{-}L + L \overset{K_2}{\rightleftharpoons} D\text{-}L_2 \quad (4)$$

$$D + 2L \overset{K_1K_2}{\rightleftharpoons} D\text{-}L_2 \quad (5)$$

where D is the rHSA dimer and L represents the ligand. The apparent binding constants (K_1K_2) of the warfarin and diazepam to the dimer were calculated to be 9.2×10^{10} and 3.0×10^{10} M^{-2}, respectively. If the each albumin unit independently accommodates one ligand, we estimated K_1 ($=K_2$) of each ligand as the square root of these values; 3.0×10^5 and 1.7×10^5 M^{-1}, respectively. They are almost in the same range as the binding constants for the monomeric rHSA (K_1), 3.8×10^5 and 1.4×10^5 M^{-1}, which means that neither the prevention nor the cooperation of the second ligand binding occurred in the dimer.

The attempt to prepare single crystals of the rHSA dimer for X-ray structural analysis failed, probably because it is likely to be very flexible at the BMH moiety. Transmission electron microscopy of the negatively stained samples showed homogeneous round particles with a diameter of 15–20 nm (not shown), however, the image is too small to obtain precise morphological information about the molecule.

The primary physiological function of HSA is the maintenance of COP within the blood vessels. Although HSA accounts for only 60% of the mass of the plasma protein, it contributes 80% of the COP. Two-thirds of this COP is simply the van't Hoff pressure and the other third arises from the Donnan effect of the negative charges of the plasma proteins, which is essentially due to albumin [1]. The relationship between the protein concentration and COP was observed for the rHSA and rHSA dimer solutions (Fig. 5). Both lines deviated upward from the linear correlation, because of the relatively larger value of the second virial coefficient, which is an index of the COP capacity, of the albumin molecule compared to those of the other plasma proteins. The measured rHSA monomer's curve coincided well to the previously reported result of Scatchard and co-workers (dotted line) [29]. The physiological concentration (5 g dL^{-1}) of rHSA represented the COP of 19 Torr. The careful inspections of their COP curves revealed that the 8.5 g dL^{-1} dimer solution has the same COP as the 5 g dL^{-1} rHSA. The plots of [C] versus COP/[C] gave a straight line, and the extrapolations to the y intercept afford the molecular weights of the monomer and dimer of 66×10^3 and 136×10^3 Da, respectively.

3.3. Viscosity and compatibility with blood components

Viscosity is a characteristic of proteins related to their size, shape, and conformation. The PBS solution of 8.5 g dL^{-1} rHSA dimer exhibited a Newtonian flow similar to the 5.0 g dL^{-1} rHSA, and showed a viscosity of 1.2 cP at a shear rate of 230 s^{-1} (Fig. 6). The dimer solution was then mixed with freshly drawn whole blood (1:1, v/v). The obtained suspension did not show any coagulation or precipitation for 6 h at 37 °C (after 6 h, hemolysis gradually took place even in the control experiment with saline or rHSA), and its viscosity profile was again Newtonian (1.8 cP at 230 s^{-1}). This result demonstrated good compatibility of the rHSA dimer with blood.

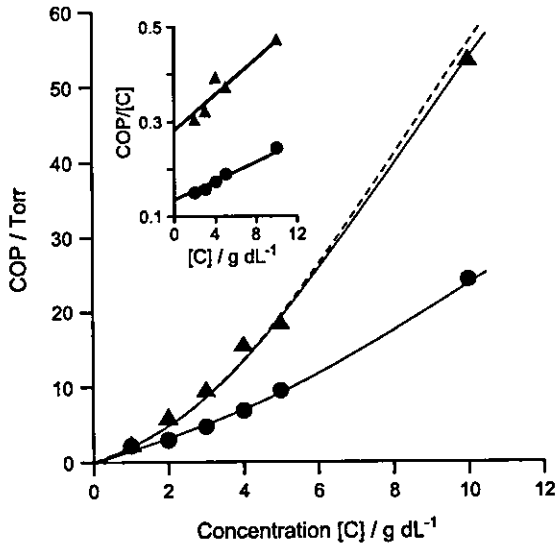

Fig. 5. Concentration [C] dependence of COP of rHSA monomer (▲) and rHSA dimer (●) in PBS (pH 7.4) at 22 °C. The dotted line represents the plasma HSA results taken from Ref. [29]. Inset shows relationship between [C] and COP/[C] for rHSA monomer (▲) and rHSA dimer (●).

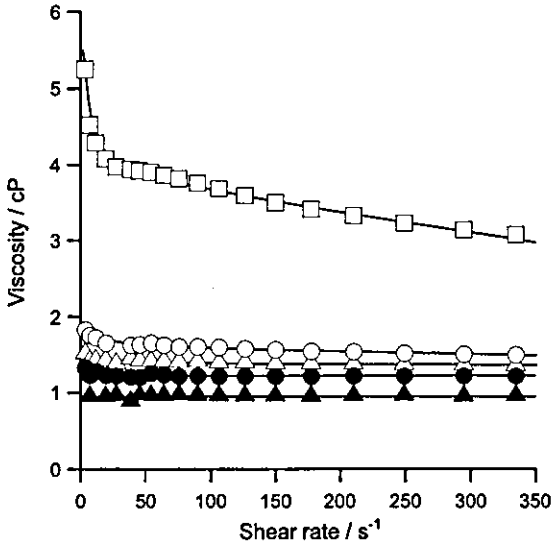

Fig. 6. Changes in the viscosity of rHSA monomer and rHSA dimer at various shear rates at 37 °C [□: whole blood, ●: 8.5 g dL^{-1} rHSA dimer, ▲: 5.0 g dL^{-1} rHSA, ○: 8.5 g dL^{-1} rHSA dimer plus whole blood (1:1, v/v), △: 5.0 g dL^{-1} rHSA plus whole blood (1:1, v/v)].

In order to evaluate the blood compatibility of the 8.5 g dL^{-1} rHSA dimer solution in detail, the changes in the number of blood cell components [RBC, white blood cells (WBC), and platelets (PLT)] have been counted after the mixture (1:1, v/v). The numbers just after the addition of the rHSA dimer to the whole blood were reasonably reduced to half the basal values; the same behavior was observed in the control experiments with the saline or 5 g dL^{-1} rHSA [Fig. 7(A)]. Optical microscopic observations revealed that the homogeneous round shape of the RBCs was completely retained [Fig. 7(B)(C)]. Therefore, it can be considered that no specific interaction occurred between the rHSA dimer and the blood cell components in vitro.

3.4. Immunogenicity

We then analyzed the immunological reactivity of the rHSA dimer against the anti-HSA polyclonal antibody. The absorption intensity of the reactant plate with the dimer showed clear concentration dependence in the same manner as those of the rHSA and plasma HSA groups (Fig. 8). It is known that HSA has five major antigenic sites by analysis using synthetic peptides [30,31]. The sites are nearly α-helical regions in the HSA molecule and include charged and/or aromatic residues which are important for the presentation of antigenic determinations. We previously reported that the cross-reactivity of the anti-HSA polyclonal antibody to BSA was extremely low, despite their homologies of the sequences over 70% and its antigenic sites in the same regions [32]. The antigenic epitopes of rHSA are preserved after bridging the Cys-34.

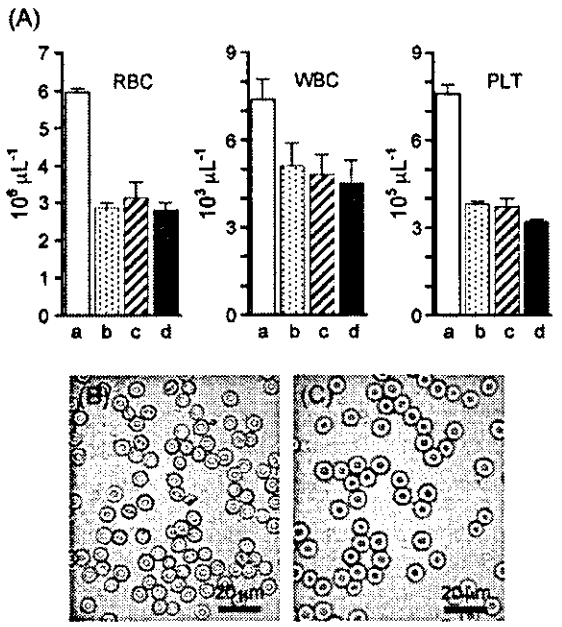

Fig. 7. (A) The blood cell (RBC, WRC, PLT) numbers in the blood suspension with the rHSA samples (1:1, v/v) at 25 °C [a: whole blood (basal value), b: with saline, c: with 5.0 g dL^{-1} rHSA, d: with 8.5 g dL^{-1} rHSA dimer]. Optical microscopic observations of (B) whole blood and (C) the blood suspension with the 8.5 g dL^{-1} rHSA dimer (1:1, v/v) (bar: 20 μm). The shape of the RBC with a diameter of ca. 8 μm did not change.

3.5. Circulation lifetime of ^{125}I-labeled rHSA dimer in rats

The rHSA and rHSA dimer labeled with ^{125}I were injected into rats to determine their blood circulation

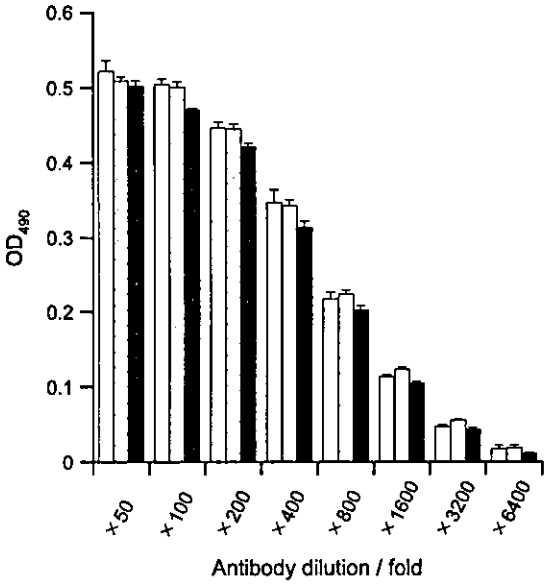

Fig. 8. Cross-reactivity of the anti-HSA polyclonal antibody with rHSA monomer and rHSA dimer [white bar: plasma HSA, diagonal bar: rHSA monomer, black bar: rHSA dimer]. All values are mean±S.D. (n=3).

tissue (P_{O_2}: 40 Torr) (23%) becomes slightly higher than that of the human RBC (22%).

4. Conclusions

The obvious characteristics of the rHSA dimer cross-linked with the bola-shaped bismaleimide are as follows: (i) unaltered essential properties of the albumin units (the secondary/tertiary structure, surface net charges, thermostability), (ii) excess ligand-binding capacity relative to the monomer while maintaining its COP at the physiological value, (iii) good blood compatibility and identical antigenic epitopes with the monomer, and (iv) longer half-life in the bloodstream and similar tissue distributions with rHSA. Furthermore, (v) one molecule of the rHSA dimer incorporates 16 FecycPs, which is exactly twice the amount compared to that of the monomeric rHSA, and the obtained hemoprotein can reversibly bind and release O_2 under physiological conditions. (vi) The 8.5 g dL^{-1} rHSA–FecycP dimer solution satisfies the initial clinical requirements for the O_2-carrier as an RBC substitute, which transports 10 mM O_2 (compared to 9.2 mM in the human blood) while maintaining the COP at a constant 19 Torr.

Acknowledgements

This work was partially supported by Grant-in-Aid for Scientific Research (no. 16350093) from JSPS, and Grant-in-Aid for Exploratory Research (no. 16655049) from MEXT Japan, and Health Science Research Grants (Regulatory Science) from MHLW Japan.

References

[1] T. Peters Jr., All about Albumin. Biochemistry, Genetics, and Medical Applications, Academic Press, San Diego, 1996, and reference therein.
[2] D.C. Carter, J.X. Ho, Structure of serum albumin, Adv. Protein Chem. 45 (1994) 153–203.
[3] S. Curry, P. Brick, N.P. Franks, Fatty acid binding to human serum albumin: new insights from crystallographic studies, Biochim. Biophys. Acta 1441 (1999) 131–140.
[4] S. Sugio, A. Kashima, S. Mochizuki, M. Noda, K. Kobayashi, Crystal structure of human serum albumin at 2.5 Å resolution, Protein Eng. 12 (1999) 439–446.
[5] DJ. Meyer, H. Kramer, N. Özer, B. Coles, B. Ketterer, Kinetics and equiliburia of *S*-nitrosothiol–thiol exchange between glutathione, cysteine, penicillamines and serum-albumin, FEBS Lett. 345 (1994) 177–180.
[6] T. Peters Jr., Serum albumin, Adv. Protein Chem. 37 (1985) 161–245.
[7] a W.L. Hughes, The proteins of blood plasma, in: H. Neurath, K. Bailey (Eds.), The Proteins, vol. IIB, Academic Press, New York, 1954, pp. 663–734;
b W.L. Hughes, H.M. Dintzis, Crystallization of the mercury dimers of human and bovine mercaptalbumin, J. Biol. Chem. 239 (1964) 845–849.
[8] R. Straessle, A disulfide dimer of human mercaptalbumin, J. Am. Chem. Soc. 76 (1954) 3138–3142.
[9] L.-O. Anderson, Hydrolysis of disulfide bonds in weakly alkaline media II. Bovine serum albumin dimer, Biochim. Biophys. Acta 117 (1966) 115–133.
[10] C.N. Cornell, R. Chang, L.J. Kaplan, The environment of the sulfhydryl group in human plasma albumin as determined by spin labeling, Arch. Biochem. Biophys. 209 (1981) 1–6.
[11] T. Komatsu, K. Hamamatsu, E. Tsuchida, Cross-linked human serum albumin dimer incorporating sixteen (tetraphenylporphinato)iron(II) derivatives: synthesis, characterization, and O_2-binding property, Macromolecules 32 (1999) 8388–8391.
[12] (a) E. Tsuchida, T. Komatsu, Y. Matsukawa, K. Hamamatsu, J. Wu, Human serum albumin incorporating tetrakis(*o*-pivalamido)phenylporphinatoiron(II) derivative as a totally synthetic O_2-carrying hemoprotein, Bioconj. Chem. 10 (1999) 797–802;
(b) T. Komatsu, Y. Matsukawa, E. Tsuchida, Kinetics of CO and O_2 binding to human serum albumin–heme hybrid, Bioconj. Chem. 11 (2000) 772–776;
(c) T. Komatsu, Y. Matsukawa, E. Tsuchida, Reaction of nitric oxide with synthetic hemoprotein, human serum albumin incorporating tetraphenylporphinatoiron(II) derivatives, Bioconj. Chem. 12 (2001) 71–75;
(d) T. Komatsu, Y. Matsukawa, E. Tsuchida, Effect of heme structure on O_2-binding properties of human serum albumin–heme hybrids: intramolecular histidine coordination provides a stable O_2–adduct complex, Bioconj. Chem. 13 (2002) 397–402.
[13] (a) E. Tsuchida, T. Komatsu, K. Hamamatsu, Y. Matsukawa, A. Tajima, A. Yoshizu, Y. Izumi, K. Kobayashi, Exchange transfusion of albumin–heme as an artificial O_2-infusion into anesthetized rats: physiological responses, O_2-delivery and reduction of the oxidized hemin sites by red blood cells, Bioconj. Chem. 11 (2000) 46–50;
(b) Y. Huang, T. Komatsu, A. Nakagawa, E. Tsuchida, S. Kobayashi, Compatibility in vitro of albumin–heme (O_2-carrier) with blood cell components, J. Biomed. Mater. Res. 66A (2003) 292–297;
(c) E. Tsuchida, T. Komatsu, Y. Matsukawa, A. Nakagawa, H. Sakai, K. Kobayashi, M. Suematsu, Human serum albumin incorporating synthetic heme: red blood cell substitute without hypertension by nitric oxide scavenging, J. Biomed. Mater. Res. 64A (2003) 257–261.
[14] E. Tsuchida, T. Komatsu, K. Arai, H. Nishide, Synthesis and O_2-binding properties of tetraphenylporphyrinatoiron(II) derivatives bearing a proximal imidazole covalently bound at the β-pyrrolic position, J. Chem. Soc., Perkin Trans. 2 1995 (1995) 747–753.
[15] B.T. Doumas, W.A. Watson, H.G. Biggs, Albumin standards and measurement of serum albumin with bromcresol green, Clin. Chim. Acta 31 (1971) 87–96.
[16] H. Watanabe, K. Yamasaki, U. Kragh-Hansen, S. Tanase, K. Harada, A. Suenaga, M. Otagiri, In vivo and in vitro properties of recombinant human serum albumin from *Pichia pastoris* purified by a method of short processing time, Pharm. Res. 18 (2001) 1775–1781.
[17] J.P. Collman, J.I. Brauman, B.L. Iverson, J.L. Sessler, R.M. Morris, Q.H. Gibson, O_2 and CO Binding to iron(II) porphyrins: a comparison of the "picket fence" and "pocket" porphyrins, J. Am. Chem. Soc. 105 (1983) 3052–3064.
[18] T.G. Traylor, S. Tsuchiya, D. Campbell, M. Mitchell, D. Stynes, N. Koga, Anthracene heme cyclophanes: steric effects in CO, O_2, and RNC binding, J. Am. Chem. Soc. 107 (1985) 604–614.
[19] E. Tsuchida, T. Komatsu, K. Arai, H. Nishide, Synthesis and dioxygen-binding properties of double-sided porphyrinatoiron(II) complexes bearing covalently bound axial imidazole, J. Chem. Soc., Dalton Trans. 1993 (1993) 2465–2469.
[20] E. Katchalski, G.S. Benjamin, V. Gross, The availability of the disulfide bonds of human and bovine serum albumin and of bovine g-globulin to reduction by thioglycolic acid, J. Am. Chem. Soc. 79 (1957) 4096–4099.

[21] D.R. Grassetti, J.F. Murray Jr., Determination of sulfhydryl groups with 2,2′ - or 4,4′ -dithiopyridine, Arch. Biochem. Biophys. 119 (1967) 41–49.
[22] A.O. Pedersen, J. Jacobsen, Reactivity of the thiol group in human and bovine albumin at pH 3–9, as measured by exchange with 2,2′ - dithiodipyridine, Eur. J. Biochem. 106 (1980) 291–295.
[23] E.J. Cohn, The properties and functions of the plasma proteins, with a consideration of the methods for their separation and purification, Chem. Rev. 28 (1941) 395–417.
[24] I. Sjöholm, I. Ljungstedt, Studies on the tryptophan and drug-binding properties of human serum albumin fragments by affinity chromatography and circular dichroism measurements, J. Biol. Chem. 248 (1973) 8434–8441.
[25] A. Sumi, W. Ohtani, K. Kobayashi, T. Ohmura, K. Yokoyama, N. Nishida, T. Suyama, Purification and physicochemical properties of recombinant human serum albumin, in: C. Rivat, J.-F. Stoltz (Eds.), Biotechnology of Blood Proteins, vol. 227, John Libbey Eurotext, Montrouge, 1993, pp. 293–298.
[26] S. Gumpen, P.O. Hegg, H. Martens, Thermal stability of fatty acid–serum albumin complexes studies by differential scanning calorimetry, Biochim. Biophys. Acta 574 (1979) 189–196.
[27] T. Kosa, M. Maruyama, M. Otagiri, Species differences of serum albumins: II. Chemical and thermal stability, Pharm. Res. 15 (1998) 449–454.
[28] a G. Sudlow, D.J. Birkett, D.N. Wade, The Characterization of two specific drug binding sites on human serum albumin, Mol. Pharmacol. 11 (1975) 824–832;
b G. Sudlow, D.J. Birkett, D.N. Wade, Further characterization of specific drug binding sites on human serum albumin, Mol. Pharmacol. 12 (1976) 1052–1061.
[29] G. Scatchard, A.C. Batchelder, A. Brown, Chemical, clinical, and immunological studies on the products of human plasma fractionation: VI. The osmotic pressure of plasma and of serum albumin, J. Clin. Invest. 23 (1944) 165–170.
[30] S. Sakata, M.Z. Atassi, Immunochemistry of serum albumin. X. Five major antigenic sites of human serum albumin are extrapolated from bovine albumin and confirmed by synthetic peptides, Mol. Immunol. 17 (1980) 139–142.
[31] C. Lapresle, N. Doyen, Studies of an antigenic site of human-serum albumin with monoclonal-antibodies, Mol. Immunol. 20 (1983) 549–555.
[32] W. Ohtani, Y. Nawa, K. Takeshima, H. Kamuro, K. Kobayashi, T. Ohmura, Physicochemical and immunochemical properties of recombinant human serum albumin from *Pichia pastoris*, Anal. Biochem. 256 (1998) 56–62.
[33] T.R. McCurdy, S. Gataiance, L.J. Eltringham-Smith, WP. Sheffield, A covalently linked recombinant albumin dimer is more rapidly cleared in vivo than are wild-type and mutant C34A albumin, J. Lab. Clin. Med. 143 (2004) 115–124.
[34] a J.P. Collman, J.I. Brauman, K.M. Doxsee, T.R. Halbert, E. Bunnenberg, R.E. Linder, G.N. LaMar, J.D. Guadio, G. Lang, K. Spartalian, Synthesis and characterization of "tailed picket fence" porphyrins, J. Am. Chem. Soc. 102 (1980) 4182–4192;
b J.P. Collman, F. Basolo, E. Bunnenberg, T.C. Collins, J.H. Dawson, P.E. Ellis Jr., M.L. Marrocco, A. Moscowitz, J.L. Sessler, T. Szymanski, Use of magnetic circular dichroism to determine axial ligation for some sterically encumbered iron(II) porphyrin complexes, J. Am. Chem. Soc. 103 (1981) 5636–5648;
c J.P. Collman, J.I. Brauman, T.J. Collins, B.L. Iverson, G. Lang, R.B. Pettman, J.L. Sessler, M.A. Walters, Synthesis and characterization of the "pocket" porphyrins, J. Am. Chem. Soc. 105 (1983) 3038–3052.
[35] J. Geibel, J. Cannon, D. Campbell, T.G. Traylor, Model compounds for R-state and T-state hemoglobins, J. Am. Chem. Soc. 100 (1978) 3575–3585.
[36] C.A. Sawicki, Q.H. Gibson, Properties of the T state of human oxyhemoglobin studied by laser photolysis, J. Biol. Chem. Soc. 252 (1977) 7538–7547.

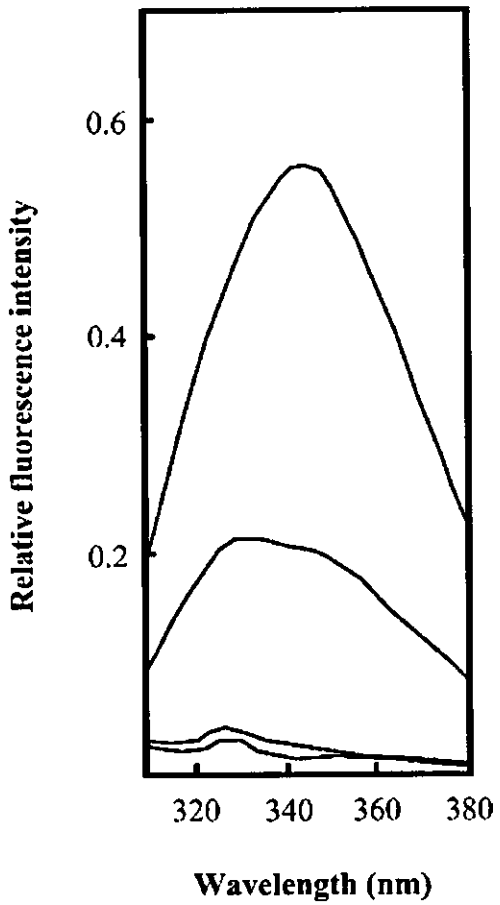

Fig. 2. Intrinsic fluorescence spectra of rHSA and individual domains. The protein concentration was 6 μM in 67 mM phosphate buffer (pH 7.4 and 25°C). From top to bottom, spectra for rHSA, domain II, domain III, and domain I.

buffer (pH 7.4), and a similar difference in activity was observed for domain II. However, this pattern of activity was not observed for the other two domains.

In order to confirm the involvement of domain II in the enolase-like activity of HSA, the enolase-like activity of rHSA (5 μM) for DHT (2 μM, 0.4 μCi) was measured in the presence of warfarin or ketoprofen (20 μM). No inhibition was observed in the presence of ketoprofen at pH 7.4 or 9.4. In contrast, in the presence of warfarin, a decrease in activity

Table II. Binding of Ketoprofen and DNSS to rHSA and Individual Domains

HSA	Percentage bound (%)	
	Ketoprofen	DNSS
rHSA	80.17 ± 6.73	62.43 ± 5.38
Domain I	6.07 ± 3.95[a,b]	4.21 ± 2.90[a,b]
Domain II	4.58 ± 1.61[a,b]	7.02 ± 2.87[a,b]
Domain III	64.00 ± 5.83[a]	38.92 ± 7.78[a]

The sample solutions contained 2.5 μM ketoprofen or DNSS and 5 μM rHSA or individual domains in 67 mM phosphate buffer (pH 7.4 and 25°C). All values are mean ± SD (n = 3 to 5).
[a] $p < 0.01$ vs. rHSA.
[b] $p < 0.01$ vs. domain III.

Table III. Hydrolysis Rate Constants (k_{obs}) for *p*-Nitrophenyl Acetate

HSA	k_{obs} ($s \times 10^{-3}$)
rHSA	7.13 ± 0.90
Domain I	1.73 ± 0.65[a]
Domain II	ND
Domain III	3.18 ± 0.83[a,b]

The reaction mixtures contained 5 μM *p*-nitrophenyl acetate and 20 μM rHSA or individual domains in 67 mM phosphate buffer (pH 7.4 and 25°C). All values are mean ± SD (n = 5 to 7). ND, not detectable.
[a] $p < 0.01$ vs. rHSA.
[b] $p < 0.01$ vs. domain I.

of about 35% was observed at pH 7.4, whereas no significant inhibition was observed at pH 9.4 (data not shown). These results suggest that the active site in site I is functional at pH 7.4, and that a new site different from site I is formed in domain II at pH 9.4, a process which is thought to be influenced by fragmentation.

Antioxidant Activity of the Recombinant HSA Domains

We examined the ability of each domain to inhibit the oxidation of DRD by H_2O_2. The RD generated by oxidation was used as an indicator of antioxidant activity (25). Figure 3 shows the capacity of rHSA and individual domains to quench DRD oxidation by H_2O_2. Domains II and III showed a weak inhibitory effect compared with rHSA, but the quenching capacity of domain I was comparable to that of rHSA.

In Vivo Studies

To evaluate whether fragmentation of domains affects the biologic fate of rHSA, we measured uptake clearance of rHSA and the corresponding domain proteins in mice (Table V). There was about a 50-fold difference in total clearance between rHSA and individual domains. However, there was no significant difference in total clearance among the domains. The three domains were mainly distributed in the kidney. However, domain III was found at slightly higher levels than other domains in the liver.

Table IV. Enolase-like Activity of rHSA and Individual Domains in Two Different Buffer Solutions

HSA	Phosphate buffer pH 7.4 (CPM)	Carbonate buffer pH 9.2 (CPM)
rHSA	5073 ± 1422	11650 ± 1374
Domain I	1467 ± 205[a]	1804 ± 36[a,b]
Domain II	727 ± 80[a]	5851 ± 1320[a]
Domain III	1110 ± 261[a]	1897 ± 171[a,b]

5 μM rHSA or individual domains was incubated with DHT (20 μM, 0.4 μCi) for 90 minutes and enzymatic activity was measured at 37°C. All values are the mean ± SD (n = 3).
[a] $p < 0.01$ vs. rHSA.
[b] $p < 0.01$ vs. domain II.

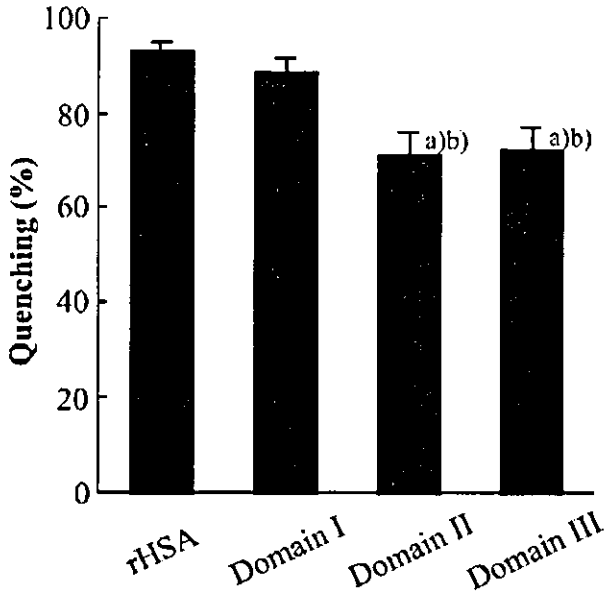

Fig. 3. Quenching of H_2O_2 oxidation of DRD by rHSA and individual domains. The sample solutions contained 7.5 μM rHSA or individual domains in 67 mM sodium phosphate buffer (pH 7.4 and 25°C), 5 μM DRD, and 25 mM H_2O_2. Each bar represents the mean ± SD (n = 3). a) $p < 0.01$ vs. rHSA; b) $p < 0.01$ vs. domain I.

DISCUSSION

The effectiveness of recombinant protein pharmaceuticals is heavily dependent on the intrinsic pharmacokinetics of the natural protein. For example, the efficacy of a drug is affected by its serum half-life. A variety of strategies have been proposed to create long-acting forms of drugs. One approach involves modification of drug formulation so that the product is slowly released from the injection site. This sustained release form requires fewer injections. However, the active agent is not changed, so elimination of the drug remains unchanged and the drug dose must be increased to cover the longer dosing interval. Another strategy is to exploit plasma protein binding; for example, noncovalent association with albumin extends the half-life of short-lived proteins. The drug is covalently linked with a component that is known to bind with high affinity to a plasma protein. Recombinant fusion of the albumin-binding domain of streptococcal protein G (which selectively binds to albumin with high affinity) to human complement receptor type 1 has been shown to increase the half-life of this receptor 3-fold to 5 h in rats (26). In another study, when insulin was acylated with myristic acids, its effects were prolonged due to its spontaneous association with albumin (27). Another approach is to modify the drug itself, so that the active drug is cleared more slowly from the systemic circulation. Because the kidney generally filters out molecules smaller than 60 kDa, efforts to reduce clearance have focused on increasing the molecular size of drugs through protein fusion, glycosylation or addition of polyethylene glycol polymers (*i.e.* PEG). Another approach is conjugation of the drug to a carrier protein to form a prodrug (5,28,29).

One of the challenges for the successful commercialization of therapeutic proteins is to maintain the safety and efficacy of the protein during its manufacturing, storage and administration. To achieve this, the purified form of the protein drug is usually formulated with carefully selected excipients. The formulation of a peptide drug preparation would require the inclusion of an antioxidant to maintain the potency of the drug as well as a lyoprotectant. A protein carrier that possesses considerable antioxidant activity could eliminate or reduce use of antioxidants in the formulation. A protein drug carrier with low or no enzymatic activity would promote the stability of a peptide drug or the peptide linker during storage, and may eliminate the need for refrigeration during storage. Low ligand binding capacity of a protein carrier may prevent accumulation of endogenous or exogenous substances which may modify the drug properties during the preparation stage or upon administration into the general circulation. Because proteins have complex molecular structures that can influence the protein stability, the development of stable formulations of protein pharmaceuticals requires an intimate knowledge of the protein structure as well as its chemical and physical properties. In particular, an understanding of the mechanisms by which a protein may degrade is crucial for designing and testing drug formulations. The major pathways of protein degradation include denaturation, aggregation, oxidation and interfacial damage.

Table V. Clearance of ^{111}In-Labeled rHSA and Individual Domains

HSA	Clearance (μl/min)		
	Total	Liver	Kidney
rHSA	3.65 ± 0.78	0.69 ± 0.21	0.28 ± 0.10
Domain I	178.35 ± 9.72[a]	5.12 ± 0.98[b,c]	147.33 ± 10.57[a]
Domain II	181.37 ± 12.12[a]	5.20 ± 2.52[c]	173.38 ± 12.35[a,d]
Domain III	184.80 ± 15.21[a]	19.09 ± 4.16[a]	171.14 ± 5.63[a,d]

All values are mean ± SD (n = 3).
[a] $p < 0.01$ vs. rHSA.
[b] $p < 0.05$ vs. rHSA.
[c] $p < 0.01$ vs. domain III.
[d] $p < 0.05$ vs. domain I.

Ligand Binding Properties

HSA is the most abundant plasma protein, and is involved in a variety of physiologic functions including maintenance of colloid osmotic pressure. One of its prominent physiologic functions is ligand transport. HSA has at least two distinct binding sites for several physiologically important compounds and a large number of hydrophobic drugs. These two major binding regions, site I and II, are located within specialized cavities in subdomain IIA and IIIA, respectively (1). Although mapping of the locations of each drug binding site had been attempted in qualitative ligand binding studies involving induced circular dichroism using recombinant domains by Dockal *et al.*, quantitative data has not been obtained.

In the current study, all domains showed a significant decrease in the percentage of ligand bound for all site I probes, compared with rHSA, except for the binding of *n*-butyl *p*-AB, a site Ic ligand that binds to domain II. It appears highly likely that the observed marked loss of the ligand binding ability of domain II, which contains site I, is due to the absence of the neighboring domain, which indicates the importance of interdomain interactions for maintaining the

26. S. C. Makrides, P. A. Nygren, B. Andrews, P. J. Ford, K. S. Evans, E. G. Hayman, H. Adari, H. Adari, M. Uhlen, and C. A. Toth. Extended *in vivo* half-life of human soluble complement receptor type 1 fused to a serum albumin-binding receptor. *J. Pharmacol. Exp. Ther.* **277**:534–542 (1996).
27. P. Kurtzhals, S. Havelund, I. Jonassen, B. Kiehr, U. D. Larsen, U. Ribel, and J. Markussen. Albumin binding of insulins acylated with fatty acids: characterization of the ligand-protein interaction and correlation between binding affinity and timing of the insulin effect *in vivo*. *Biochem. J.* **312**:725–731 (1995).
28. L. Beljaars, G. Molema, B. Weert, H. Bonnema, P. Olinga, G. M. Groothuis, D. K. Meijer, and K. Poelstra. Albumin modified with mannose 6-phosphate: A potential carrier for selective delivery of antifibrotic drugs to rat and human hepatic stellate cells. *Hepatology* **29**:1486–1493 (1999).
29. H. Sakai, S. Takeoka, S. I. Park, T. Kose, H. Nishide, Y. Izumi, A. Yoshizu, K. Kobayashi, and E. Tsuchida. Surface modification of hemoglobin vesicles with poly(ethylene glycol) and effects on aggregation, viscosity, and blood flow during 90% exchange transfusion in anesthetized rats. *Bioconjug. Chem.* **8**:23–30 (1997).
30. T. Kjeldsen, A. F. Pettersson, L. Drube, P. Kurtzhals, I. Jonassen, S. Havelund, P. H. Hansen, and J. Markussen. Secretory expression of human albumin domains in *Saccharomyces cerevisiae* and their binding of myristic acid and an acylated insulin analogue. *Protein Expr. Purif.* **13**:163–169 (1998).
31. E. Suzuki, K. Yasuda, N. Takeda, S. Sakata, S. Era, K. Kuwata, M. Sogami, and K. Miura. Increased oxidized form of human serum albumin in patients with diabetes mellitus. *Diabetes Res. Clin. Pract.* **18**:153–158 (1992).
32. W. P. Sheffield, J. A. Marques, V. Bhakta, and I. J. Smith. Modulation of clearance of recombinant serum albumin by either glycosylation or truncation. *Thromb. Res.* **99**:613–621 (2000).
33. K. Nakajou, H. Watanabe, U. Kragh-Hansen, T. Maruyama, and M. Otagiri. The effect of glycation on the structure, function and biological fate of human serum albumin as revealed by recombinant mutants. *Biochim. Biophys. Acta* **1623**:88–97 (2003).

THE JOURNAL OF BIOLOGICAL CHEMISTRY
Vol. 280, No. 2, Issue of January 14, pp. 1384–1391, 2005
Printed in U.S.A.

Use of Photoaffinity Labeling and Site-directed Mutagenesis for Identification of the Key Residue Responsible for Extraordinarily High Affinity Binding of UCN-01 in Human α1-Acid Glycoprotein*

Received for publication, September 27, 2004, and in revised form, October 26, 2004
Published, JBC Papers in Press, October 27, 2004, DOI 10.1074/jbc.M411076200

Masaaki Katsuki‡, Victor Tuan Giam Chuang‡§, Koji Nishi‡, Kohichi Kawahara¶, Hitoshi Nakayama¶, Noriyuki Yamaotsu‖, Shuichi Hirono‖, and Masaki Otagiri‡**

From the Departments of ‡Biopharmaceutics and ¶Molecular Cell Function, Graduate School of Medical and Pharmaceutical Sciences, Kumamoto University, 5-1 Oe-honmachi, Kumamoto, 862-0973, Japan, the §Department of Pharmacy, Faculty of Allied Health Sciences, Universiti Kebangsaan Malaysia, Jalan Raja Muda Abdul Aziz, 50300 Kuala Lumpur, Malaysia, and ‖The School of Pharmaceutical Sciences, Kitasato University, 5-9-1, Shirokane, Minato-ku, Tokyo, 108-8641, Japan

7-Hydroxystaurosporine (UCN-01) is a protein kinase inhibitor anticancer drug currently undergoing a phase II clinical trial. The low distribution volumes and systemic clearance of UCN-01 in human patients have been found to be caused in part by its extraordinarily high affinity binding to human α1-acid glycoprotein (hAGP). In the present study, we photolabeled hAGP with [^{3}H]UCN-01 without further chemical modification. The photolabeling specificity of [^{3}H]UCN-01 was confirmed by findings in which other hAGP binding ligands inhibited formation of covalent bonds between hAGP and [^{3}H]UCN-01. The amino acid sequence of the photolabeled peptide was concluded to be SDVVYTDXK, corresponding to residues Ser-153 to Lys-161 of hAGP. No PTH derivatives were detected at the 8th cycle, which corresponded to the 160th Trp residue. This strongly implies that Trp-160 was photolabeled by [^{3}H]UCN-01. Three recombinant hAGP mutants (W25A, W122A, and W160A) and wild-type recombinant hAGP were photolabeled by [^{3}H]UCN-01. Only mutant W160A showed a marked decrease in the extent of photoincorporation. These results strongly suggest that Trp-160 plays a prominent role in the high affinity binding of [^{3}H]UCN-01 to hAGP. A docking model of UCN-01 and hAGP around Trp-160 provided further details of the binding site topology.

Human α1-acid glycoprotein (hAGP)[1] is an acute phase protein with a molecular mass of 41 to 43 kDa and is heavily glycosylated (45%) (1). It contains sialic acids, which cause it to be negatively charged (pI = 2.7~3.2) (2). Its glycosylation pattern can change depending on the type of inflammation (3). The biological function of hAGP is not clear, although studies using *in vivo* models of inflammation indicate that it plays anti-inflammatory and immunomodulating roles and has protective effects (4, 5). The "basal" level of hAGP is ~20 μmol/liter, but hAGP levels can increase by 5–10-fold in response to stress, infection, or an inflammatory response to neoplasm (6, 7). In addition to increases in hAGP plasma concentration in certain cancers, changes in the expression of genetic variants of hAGP can occur according to the specific type of cancer (8). The levels of hAGP vary widely and heterogeneously among cancer patients; according to the type of disease, the composition of hAGP consists of various isoforms and degrees of glycosylation (9). Studies have shown that increases in circulating hAGP alter the pharmacokinetic disposition and pharmacological action of numerous drugs that bind to it (10–12). For example, increased hAGP levels associated with advanced tumors alter the pharmacokinetics of Imatinib (STI571), a tyrosine kinase inhibitor, in leukemia patients (13). hAGP also appears to be an independent predictor of response and a major objective prognostic factor of survival in patients with non-small cell lung cancer treated with docetaxel chemotherapy (14). Thus, hAGP is an important modulator of drug pharmacokinetics and pharmacodynamics in anticancer therapeutics.

7-Hydroxystaurosporine (UCN-01) has an indolocarbazole moiety and was originally isolated as a selective inhibitor of a Ca^{2+}- and phospholipid-dependent protein kinase (protein kinase C (PKC)) (15). UCN-01 is a derivative of staurosporine, which occurs naturally, inhibits numerous other kinases, and has greater selectivity for PKC than does staurosporine (16, 17). UCN-01 can mediate 3 distinct cellular effects *in vitro*: cell cycle arrest, induction of apoptosis, and potentiation of DNA damage-related toxicity (18–20). It exhibits anticancer activity against human and murine tumor cell lines that have aberrations in cellular signal transduction (21–24). Unlike other compounds with an indolocarbazole moiety, UCN-01 preferentially induces G_1 phase accumulation in various cell lines, and one of its mechanisms of action is clearly mediated by dephosphorylation of retinoblastoma protein and inhibition of cyclin-dependent kinase 2 (CDK2), an intracellular retinoblastoma protein kinase that regulates the transition from the G_1 to S phase (25). In addition, UCN-01 enhances the anticancer effects of several important chemotherapeutic drugs, including mitomycin C, cisplatin, and 5-fluorouracil, *in vitro* and *in vivo* (26–28). UCN-01 is currently in the phase II study of its effects on relapsed or refractory systemic anaplastic large cell and mature T-cell lymphomas (29, 30). UCN-01 was initially administered as a 72-h continuous infusion every 2 weeks, based on data from *in vitro* and xenograft preclinical models. However, in the first few patients, the drug had an unexpectedly long half-life (>30 days), which was 100 times longer than the

* The costs of publication of this article were defrayed in part by the payment of page charges. This article must therefore be hereby marked "*advertisement*" in accordance with 18 U.S.C. Section 1734 solely to indicate this fact.

** To whom correspondence should be addressed: Dept. of Biopharmaceutics, Graduate School of Pharmaceutical Sciences, Kumamoto University, 5-1 Oe-honmachi, Kumamoto, 862-0973, Japan. Tel.: 81-96-3714150; Fax: 81-96-3627690; E-mail: otagirim@gpo.kumamoto-u.ac.jp.

[1] The abbreviations used are: hAGP, human α1-acid glycoprotein; UCN-01, 7-hydroxystaurosporine; rhAGP, recombinant hAGP; PVDF, polyvinylidene difluoride; HPLC, high performance liquid chromatography; PKC, protein kinase C.

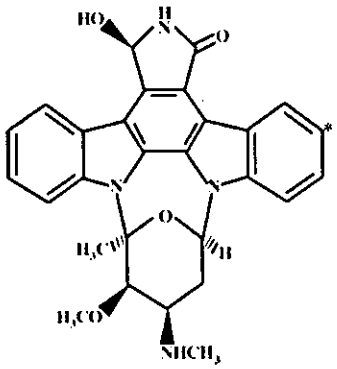

FIG. 1. **Chemical structure of [^{3}H]UCN-01.** *, ^{3}H-labeled position.

half-life observed in preclinical models. The distribution volumes (0.0796~0.158 liter/kg) and systemic clearance (0.0407~0.252 ml/h/kg) in the human patients were found to be extremely low. This pharmacokinetic behavior of UCN-01 in humans can partly be attributed to its specific high affinity binding to hAGP, which causes slow dissociation of UCN-01 from hAGP and thereby limits its disposition and elimination (31, 32). The binding constant for UCN-01 and hAGP, 8×10^8 M^{-1}, is the highest value ever reported for protein binding studies (33).

Several protein binding studies of hAGP had been conducted using a variety of techniques including equilibrium dialysis, ultrafiltration, chemical modification, and displacement (34–37). In a recent study, we identified the key factors contributing to the unusually high binding affinity between UCN-01 and hAGP: the substituent at C-7 of the UCN-01 molecule, and the Trp residues of hAGP (38). Crystallographic structural analysis has become more common and appears to be a good method for analysis of ligand-protein interaction, but there have been no reports of crystallographic structural analysis of hAGP. Certain experimental techniques allow direct evaluation of ligand-protein complexes, which can elucidate the binding chemistry of hAGP. Photoaffinity labeling is an essential complement to modeling and mutagenesis and allows direct, unambiguous identification of the contact region between a binding protein and its specific photoactivatable ligands (39–41). There is no photoaffinity labeling study that has led to the direct determination of labeled amino acid residues in hAGP. In the present study, we used [^{3}H]UCN-01 (Fig. 1) as a photoaffinity labeling agent to characterize the binding site of hAGP. Also, single residue mutants of recombinant hAGP (W25A, W122A, and W160A) were produced in order to determine which Trp was involved in the high affinity binding of [^{3}H]UCN-01. Finally, we constructed models of the docking of UCN-01 into the binding cavity, using a three-dimensional molecular model of hAGP.

EXPERIMENTAL PROCEDURES

Materials—[^{3}H]UCN-01 (12 Ci/mmol), UCN-01, UCN-02, and staurosporine were supplied by Kyowa Hakko Kogyo Co. (Shizuoka, Japan). hAGP (purified from cohn fraction VI) was purchased from Sigma. Sequencing grade modified trypsin was purchased from Promega. All other chemicals and solvents were of analytical grade. *N*-Glycosidase F recombinant (PNGase F) was purchased from Roche Applied Science. Plasma-derived AGP (pAGP), propranolol, and progesterone were purchased from Sigma. Potassium warfarin was donated by Eisai Co. (Tokyo, Japan). Restriction enzymes, *Escherichia coli* JM109, the DNA ligation kit, and the DNA polymerase Premix Taq® (EX Taq version) were obtained from Takara Biotechnology Co. Ltd. (Kyoto, Japan). The DNA sequencing kit was obtained from PerkinElmer Applied Biosystems (Tokyo, Japan). The Pichia expression kit was purchased from Invitrogen. DEAE Sephacel, phenyl-Sepharose Fast Flow, and Sephadex G-75 superfine were purchased from Amersham Biosciences.

Expression and Purification of Wild-type and Mutant rhAGP—Recombinant hAGP (rhAGP) was expressed in the methylotropic yeast *Pichia pastoris* using the expression vector pPIC9, and was purified by anionic exchange, hydrophobic interaction, and gel filtration chromatography (42). The single residue mutants W25A, W122A, and W160A were prepared using a QuikChange® XL site-directed mutagenesis kit, following the procedure of Braman *et al.* (43).

Purification of rhAGP—The growth medium was separated from the yeast by centrifugation (6000 × *g*, 10 min, 4 °C), and the secreted rhAGP was isolated from the medium as follows. The medium was brought to 60% saturation with ammonium sulfate at room temperature. The temperature was then lowered to 4 °C, and the pH was adjusted to 4.0. After shaking for 12 h, the precipitated protein was collected by centrifugation (12,000 × *g*, 60 min, 4 °C) and resuspended in distilled water. Dialysis was performed for 48 h at 4 °C against 100 volumes of distilled water, followed by a further 24 h of dialysis against 100 volumes of 10 mM Tris-HCl buffer (pH 7.4). Then, the solution was loaded onto a column of DEAE Sephacel. rhAGP was eluted with a linear gradient of 0–1 M NaCl in 10 mM Tris-HCl buffer (pH 7.4). The eluted rhAGP was loaded onto a column of phenyl-Sepharose Fast Flow. Finally, rhAGP was purified using Sephadex G-75 superfine resin.

Photoaffinity Labeling of hAGP—hAGP (50 μM) was incubated with [^{3}H]UCN-01 (0.08 μM) in 100 μl of 20 mM Tris-HCl (pH 7.4) in a 1.5-ml Eppendorf tube at room temperature in the dark for 60 min. The incubation mixture was then placed on ice and irradiated for 30 min by a 100-watt black light/blue lamp (310 nm, Ultra-Violet Products, Inc., San Gabriel, CA) at a distance of 10 cm. After irradiation, the photolabeled hAGP was precipitated by adding 1 ml of acetone, followed by centrifugation at 15 × 1000 rpm for 10 min. The pellet was washed with 1 ml of ethanol and centrifuged a second time.

SDS-PAGE and Electroblotting—Photolabeled hAGP was analyzed by SDS-PAGE using a 10% polyacrylamide gel (according to the method of Laemmli) and a sampling buffer (10 mM Tris-HCl, pH 7.6, 1% (w/v) SDS, 20 mM dithiothreitol, 4 mM EDTA, and 2% (w/v) sucrose). The concentration of protein was determined by Bradford assay using bovine serum albumin as the standard (44). After electrophoresis, the gel was electrophoretically transferred onto a PVDF membrane in a transfer buffer (25 mM Tris, 193 mM glycine, 10% methanol) using a semidry blotting assembly. The blotted membrane was stained with Coomassie Brilliant Blue R250, followed by complete drying in air.

Autoradiograpic Analysis—For autoradiographic analysis, the dried PVDF membrane was placed in contact with an imaging plate (BAS III, Fuji Photo Film Co.) in a cassette (BAS cassette 2040) at room temperature for 48 h. The imaging plate was scanned and analyzed using a Bio-Imaging Analyzer (model BAS FLA-3000 G; Fuji Photo Film Co.), and was then analyzed using L Process V1.6 software (Fuji Film Science Lab 98). The incorporation of radioactivity into individual fragments was quantified using Image Gauge V3.1 software (Fuji Film).

Competition Experiments—In order to determine the photolabeling specificity of the binding site of [^{3}H]UCN-01, hAGP (50 μM) was incubated with [^{3}H]UCN-01 (0.08 μM) in the presence of competitors (250 μM) prior to photolysis. The competitors were the UCN-01 analogues staurosporine and UCN-02, the basic drug propranolol, the acidic drug warfarin, and progesterone (representative steroid hormone). The photolabeled hAGP was separated by 10% gel SDS-PAGE and electroblotted onto a PVDF membrane before being subjected to autoradiographic analysis.

Reductive Pyridylethylation and Deglycosylation of hAGP—After the photolabeled hAGP was precipitated by acetone, 100 μl of the buffer was added to the precipitate. Then, 10 μl of 1% SDS and 1 M 2-mercaptoethanol were added to this solution, followed by reduction at 100 °C at 10 min. For deglycosylation of hAGP, 10 μl of 10% *n*-octanoyl-*N*-methylglucamide (MEGA-8), 50 μl of deionized water and 2 units of PNGase F were added to the reduction solution, and the resulting solution was incubated for 24 h. Then, 1 μl of 4-vinylpyridine was added, the mixture was further incubated in a N_2 atmosphere for 30 min at room temperature in the dark, and was then dialyzed for desalination.

Tryptic Digestion and Purification of Photolabeled hAGP Peptide Fragments—Tryptic digestion was performed in 50 mM NH_4HCO_3 (pH 7.8). After deglycosylation, deglycosylated hAGP was incubated with trypsin for 5 h at 37 °C. The ratio of trypsin to hAGP was 1:20 (w/w). Tryptic peptides were separated by reverse-phase C_{18} column (5 μm, 4.6 × 250 mm, Vydac) high performance liquid chromatography (HPLC) using an aqueous acetonitrile gradient in the presence of 0.1% trifluoroacetic acid. The separated peptides were fractionated every 30 s; 200 μl of each fraction were added to 2.5 ml of scintillation mixture; and the radioactivity was determined using a LSC-500 liquid scintillation counter (Aloka, Tokyo, Japan). The fraction with the highest radioactivity was collected in an Eppendorf tube, and was evaporated on a SpeedVac

evaporator until the volume of the sample was about 50 μl.

Capillary HPLC Separation and Sequencing—After evaporation, 10 μl of the sample was injected into an ABI 173 A MicroBlotter Capillary HPLC System (PerkinElmer Life Sciences) (45). The sample was manipulated according to the manufacturer's instructions (User's Manual, PerkinElmer Life Sciences). Meanwhile, the blotted membrane from the capillary HPLC separation using a C_{18} column (5 μm, 1.5 × 150 mm, PerkinElmer) was in contact with an imaging plate for 48 h prior to autoradiography analysis. The PVDF membrane was aligned with the chromatogram of a peptide map from the ABI 173 A MicroBlotter Capillary HPLC System. Portions of the PVDF membrane were excised for sequencing on an Applied Biosystems Procise Sequencer with reference to the autoradiogram.

Docking of UCN-01 to hAGP—The structure of hAGP has not previously been experimentally determined. As a model of the three-dimensional structure of hAGP for ligand docking, we used the modeled structure of hAGP obtained by Kopecky *et al.* (46). The initial structure of UCN-01 was taken from the crystal structure of the Chk1-UCN-01 complex (47, PDB ID 1NVQ). The docking calculation of UCN-01 to hAGP was performed using the SYBYL FlexX (48) under the condition that UCN-01 interacts with Trp-160. During the docking calculation, the structure of hAGP and the ring conformation of UCN-01 were kept rigid. The docking algorithm produced 158 different placements of UCN-01 in hAGP. All placements were evaluated by SYBYL CScore and were then ranked using AASS (Average of Auto-Scaled Scores), as follows in Equation 1.

$$\mathrm{AASS}^{\mathrm{placement}} = \left| \sum_{i} \frac{i\_Score^{\mathrm{placement}} - \min(i\_Score)}{\max(i\_Score) - \min(i\_Score)} \right| \Big/ n \qquad \text{(Eq. 1)}$$

In the AASS calculation, n = 5 and i = F_Score (48), G_Score (49), PMF_Score (50), D_Score (51), ChemScore (52). Although the top 5 placements had nearly the same AASS values, they were classified into two types of binding modes. For each type, we chose the placement with the best AASS value as the candidate binding mode. In the type I model, UCN-01 is bound to a hydrophobic pocket formed by Val-41, Ile-44, Phe-48, and Val-156. In the type II model, UCN-01 is packed into a hydrophobic pocket consisting of Ile-28, Pro-131, Leu-138, Tyr-157, and Trp-160.

Refinement of Docking Models—To refine the docking models, the coordinates of the atoms of UCN-01 and the atoms of hAGP within 10 Å from UCN-01 were optimized to reduce the root mean square of the gradients of potential energy below 0.05 kcal mol^{-1} Å-1 using SYBYL 6.9.1 (Tripos, Inc., 2003). The Tripos force field was used for the molecular energy calculation. The AMBER 7 charges (53) were used as the atomic charges for hAGP. The Gasteiger-Hückel charges (54–57) were used as the charges for UCN-01. The cut-off distance for the non-bonded interactions was 10 Å. The distance-dependent dielectric constant of 4r was used. Due to the lack of hydrogen atoms in the modeled structure of hAGP, the initial positions of the hydrogen atoms in the hAGP were generated by the SYBYL.

Statistical Analysis—Statistical analysis of differences was performed by one-way ANOVA followed by the modified Fisher's least squares difference method.

RESULTS

Photolabeling of [^{3}H]UCN-01 to hAGP—The autoradiogram in Fig. 2 shows that the band of radiolabeled protein appeared only upon the photoirradiation of hAGP with [^{3}H]UCN-01. The radioactivity band indicated the incorporation of [^{3}H]UCN-01 to hAGP via photoirradiation. No band of radiolabeled protein could be observed for the sample without irradiation indicating that no covalent attachment of [^{3}H]UCN-01 to hAGP occurred in the dark. Exposure to light for 30 min was sufficient for the photoincorporation of [^{3}H]UCN-01 to hAGP (Fig. 3). The results indicate that [^{3}H]UCN-01 is photoactivatable and stable in the dark.

Competition Experiments—In a previous study using ultracentrifugation methods, it was concluded that the binding site for UCN-01 on hAGP partly overlaps with the binding site for basic drugs, acidic drugs, and steroid hormones (58). In the present photolabeling experiment, in order to determine the photolabeling specificity of [^{3}H]UCN-01, we used staurosporine and UCN-02 (a stereoisomer of UCN-01), which also bind

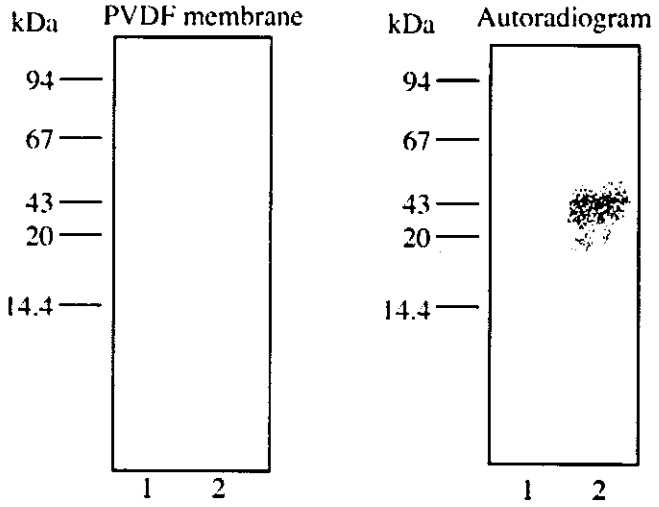

FIG. 2. **Photolabeling of hAGP with [^{3}H]UCN-01.** *Lane 1*, sample taken just prior to photoirradiation. *Lane 2*, sample taken after 30-min photoirradiation (>300 nm). 50 μM hAGP was incubated with 0.08 μM [^{3}H]UCN-01 for 60 min prior to photoirradiation. The samples were separated with 10% SDS-PAGE and electroblotted onto a PVDF membrane for autoradiographic analysis.

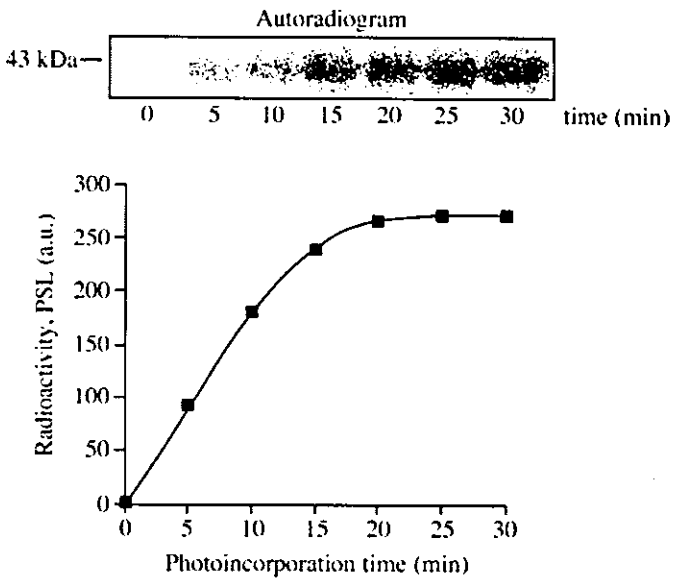

FIG. 3. **Time course of [^{3}H]UCN-01 photoincorporation.** 50 μM hAGP was incubated with 0.08 μM [^{3}H]UCN-01 for 60 min prior to photoirradiation. Aliquots of 100 μl were taken from the mixture solution at each time point as stated in the figure during irradiation until 30 min. All samples were separated with 10% SDS-PAGE and electroblotted onto a PVDF membrane for autoradiographic analysis. *PSL*, photostimulated luminescence.

hAGP, as competitors. All staurosporine analogs significantly inhibited photoincorporation, by more than 60% (Fig. 4). Other competitors that we used were representatives of other hAGP ligands: an acidic drug (warfarin), a basic drug (propranolol), and a steroid (progesterone). Warfarin and propranolol inhibited binding by less than 30%, but to a significant degree, whereas progesterone inhibited binding by about 60% (Table I).

Amino Acid Sequence of the Photolabeled Tryptic Peptides—Tryptic peptides of the hAGP photolabeled with [^{3}H]UCN-01 were separated by reverse phase HPLC using a C_{18} column. The major radioactive peptides were eluted in 10.5–11.5 min (Fig. 5, *A* and *B*). The fractions eluted within this time frame were collected and concentrated with a SpeedVac evaporator for further capillary HPLC analysis. The concentrated sample from previous HPLC analysis was separated and simulta-

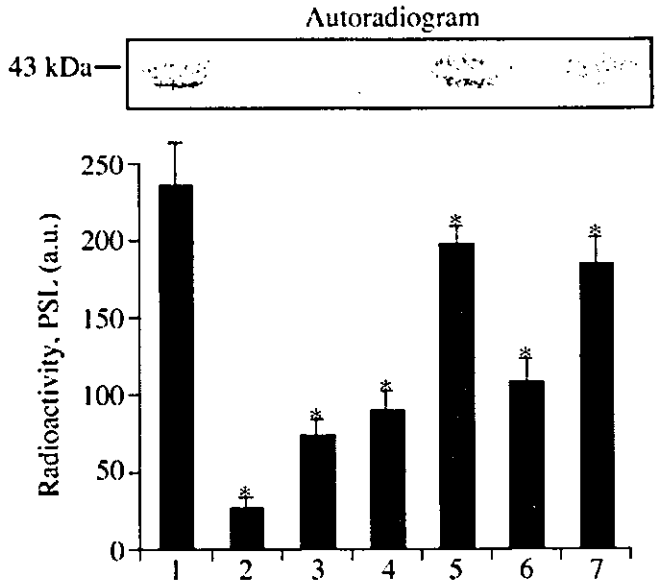

FIG. 4. **Photolabeling of hAGP with [^{3}H]UCN-01 in the presence of competitors.** *Lane 1*, no competitor; *lane 2*, cold UCN-01; *lane 3*, staurosporine; *lane 4*, UCN-02; *lane 5*, warfarin; *lane 6*, progesterone; *lane 7*, propranolol. 50 μM hAGP was incubated with 0.08 μM [^{3}H]UCN-01 and 250 μM competitors for 60 min prior to photoirradiation. The incubation mixture was irradiated for 30 min, separated with 10% SDS-PAGE, and electroblotted onto a PVDF membrane for autoradiographic analysis. *, statistically significant, compared with no competitor; $p < 0.01$. *PSL*, photostimulated luminescence.

TABLE I
Binding affinity constant and inhibition percentage by the competitors

Competitor	K_a	Inhibition
	M^{-1}	%
Cold UCN-01[a]	2.88×10^8	86.38
Staurosporine[a]	1.13×10^7	68.54
UCN-02[a]	1.48×10^6	61.52
Warfarin[b]	1.08×10^6	16.43
Progesterone[b]	1.00×10^6	58.71
Propranolol[b]	2.98×10^5	26.26

[a] Binding constant data taken from Ref. 38.
[b] Binding constant data taken from Ref 59.

neously blotted onto a strip of PVDF membrane using an ABI 173 A MicroBlotter Capillary HPLC System. Autoradiographic analysis of the PVDF membrane indicated that the radioactive spot corresponded to the peak observed at 84–85 min (Fig. 6, *A* and *B*). Edman sequencing of this spot revealed an amino acid sequence of SDVVYTDXK (Fig. 7), corresponding to Ser-153 to Lys-161 of hAGP.

Photolabeling of Wild-type and Mutant rhAGP with [^{3}H]UCN-01—Mutation of the 160th Trp residue of rhAGP to an Ala residue (W160A) caused a significant decrease in photoincorporation, by about 80%. In contrast, there was no significant difference in photoincorporation of [^{3}H]UCN-01 between wild-type rhAGP and the rhAGP mutants W25A and W122A (Fig. 8).

Docking of UCN-01 to hAGP—We constructed models of the docking of UCN-01 into the binding cavity of hAGP around Trp-160, using the three-dimensional molecular model of hAGP published by Kopecky *et al.* (46), to map the possible binding sites of hAGP. Molecular modeling calculations revealed 2 potential binding sites, type I and type II, around Trp-160, both of which were located in the outer region of hAGP (Fig. 9*A*). Table II shows the distance and nature of interaction between donors and acceptors in the models of types I and II. In the type II model, UCN-01 is packed into a surface cleft consisting of Ile-28, Pro-131, Glu-132, Lys-135, Leu-138, Tyr-157, Trp-160,

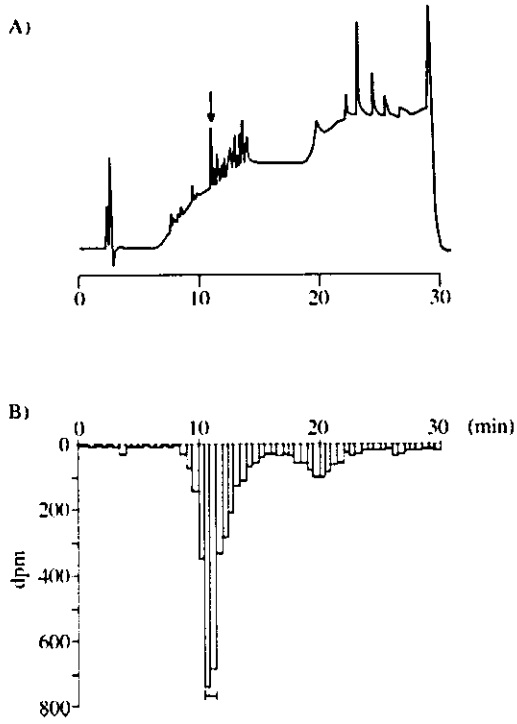

FIG. 5. **Reverse-phase HPLC separation of tryptic peptides of hAGP photolabeled with [^{3}H]UCN-01.** *A*, chromatogram of tryptic peptides of hAGP photolabeled with [^{3}H]UCN-01 detected at UV absorption wavelength of 210 nm. *B*, radioactivity of the reverse-phase fractions (200 μl) was determined by scintillation counting. An aliquot of 20 μl of the tryptic peptides was applied to a C_{18}-column and eluted at 1 ml/min using an aqueous acetonitrile gradient in the presence of 0.1% trifluoroacetic acid (from 5 to 95% acetonitrile over the course of 40 min).

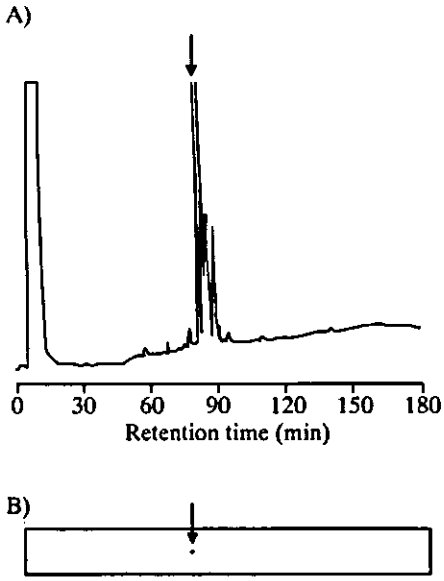

FIG. 6. **Chromatogram of capillary HPLC and autoradiogram of blotted PVDF membrane.** *A*, UV-absorption (210 nm). *B*, autoradiogram of blotted PVDF membrane. After purification of peptides using reverse-phase HPLC, an aliquot of 10 μl of the evaporating sample was applied to a C_{18} column and eluted at 5 μl/min using an aqueous acetonitrile gradient in the presence of 0.1% trifluoroacetic acid (from 5 to 95% acetonitrile over the course of 200 min). The blotted membrane from the capillary HPLC separation was in contact with an imaging plate for 48 h prior to autoradiography analysis.

and Lys-161 (Fig. 9*B*). The surrounding amino acid residues within 5 Å of the UCN-01 molecule include Lys-135, Tyr-157, Trp-160, and Lys-161. The oxygen atom in the sugar ring of

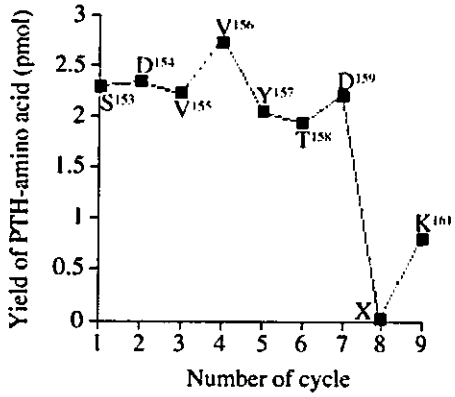

^{150}IPKSDVVYTDWKKDKC^{165}

FIG. 7. **N-terminal amino acid sequence analysis by the Edman degradation method and amino acid sequence of the photolabeled region of hAGP (tryptic peptides).** *PTH*, phenylthiohydantoin.

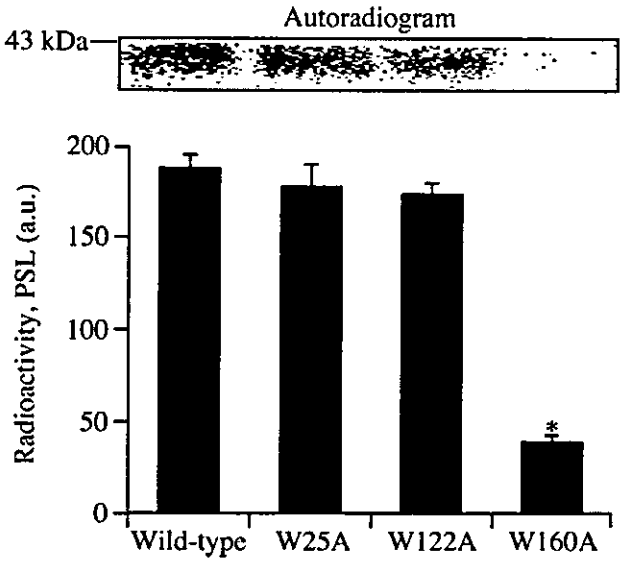

FIG. 8. **Photolabeling of wild type, W25A, W122A, and W160A with [^{3}H]UCN-01.** A sample of 50 μM rhAGP was incubated with 0.08 μM [^{3}H]UCN-01 for 60 min prior to photoirradiation. The samples were separated with 10% SDS-PAGE and electroblotted onto a PVDF membrane for autoradiographic analysis. *, statistically significant, compared with wild type; $p < 0.01$. *PSL*, photostimulated luminescence.

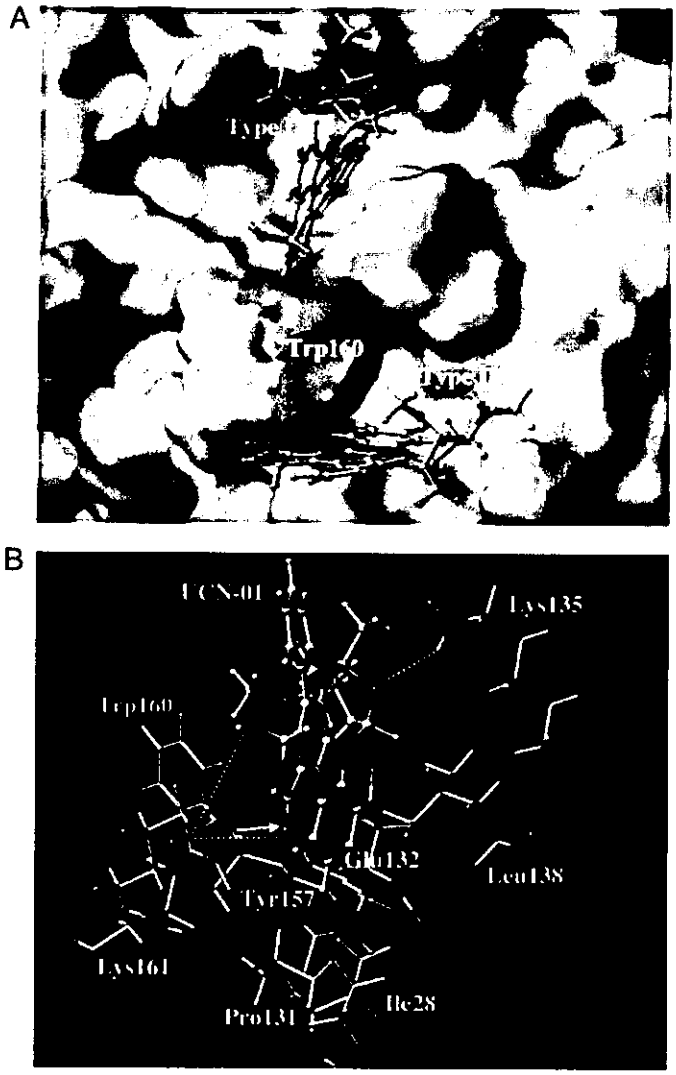

FIG. 9. *A*, type I and II docking models of UCN-01 and hAGP. Hydrophobic amino acids are shown in *green*. *B*, amino acid residues in a surface cleft around Trp-160 that interacts with UCN-01 exhibited in type II docking model. *Dotted line*, electrostatic interaction. *Arrow*, hydrogen bonding.

UCN-01 is in contact with Lys-135. The C=O group of UCN-01 was observed to form a hydrogen bond with the amino group of Trp-160, and electrostatic interaction was observed between the amino group of Lys-161 and both the 7-OH group and C=O group of UCN-01. Furthermore, the aromatic ring of UCN-01 is adjacent to Tyr-157 and Trp-160. In contrast, these interactions were not observed in the type I model, in which UCN-01 was shown to be packed into a surface cleft consisting of Val-41, Glu-43, Ile-44, Phe-48, Tyr-50, Val-156, Thr-158, and Trp-160 (data not shown).

DISCUSSION

The acute phase response alters the composition of carrier proteins in plasma, which may affect the blood deposition and transport of biomediators and drugs. Understanding the interaction of drugs with plasma proteins is essential to understanding their systemic pharmacology and toxicology. Thus, information about the effects of the acute phase response on the ligand binding ability of plasma can be used to optimize drug administration protocols in clinical practice. hAGP has been reported to be a major plasma protein that predominantly binds basic drugs (60). However, protein binding studies suggest that hAGP has 1 wide and flexible drug binding area that accommodates not only basic but also acidic and steroidal drugs (61). A current model of the hAGP binding site depicts a buried pocket with a negatively charged region that interacts with the N termini of basic drugs (62). The tertiary structure of hAGP has proven refractory to resolution, and structure-activity studies using various approaches are needed to clarify the nature of the binding site on this important protein.

The initial treatment protocol for UCN-01 was a 72-h infusion administered at 2-week intervals, because certain cell types (*e.g.* MDA-MB-468 breast carcinoma cells) required 72 h of drug exposure before irreversible growth inhibition occurred (23). However, the clinical outcome of the first 9 patients treated using this schedule demonstrated unexpectedly high concentrations of the drug with a long terminal elimination half-life ($t_{1/2}$). This led to a modification of the UCN-01 administration schedule, in which the recommended phase II dose of UCN-01 is administered as a 72-h continuous infusion at 42.5 mg/m^2/d over a 3-day period. Second and subsequent courses were administered for only 36 h at the same concentration and

TABLE II
Interaction and distance between donors and acceptors in the model of types I and II

Donor	Acceptor	Interaction	Distance
			Å
Type I			
UCN-01@NH_2^+	Glu-43@OE2	Hydrogen bonding	2.793
Tyr-50@OH	UCN-01@C=O	Hydrogen bonding	2.770
Type II			
Trp-160@NE1	UCN-01@C=O	Hydrogen bonding	2.878
Lys-135@NZ	UCN-01@-O-	Electrostatic	4.760
Lys-161@NZ	UCN-01@OH	Electrostatic	4.727
Lys-161@NZ	UCN-01@C=O	Electrostatic	4.350
Tyr-157	UCN-01	Stacking	4.204
Trp-160	UCN-01	Stacking	2.878

infusion rate, which effectively reduced the administered dose by 50% for the second and subsequent courses. In addition, the time between courses was increased from 2 weeks to 4 weeks (29). The extremely low clearance and small distribution volume of UCN-01 in humans may be partially caused by its high degree of binding to hAGP (32). Whereas many drugs that associate with hAGP have K_a values of 10^5–10^6 M^{-1}, UCN-01 is unique in its high affinity binding to hAGP, and has a K_a value of 8×10^8 M^{-1}. The results of this extraordinarily high binding affinity include a low volume of distribution (which approximates the extracellular volume) and long $t_{1/2}$ (32). The pharmacokinetic effects of the high affinity of UCN-01 for interaction with hAGP indicate that plasma levels of hAGP should be an important consideration in planning of clinical treatment. hAGP has been reported to be a major drug binding plasma protein that interacts mainly with basic drugs (63). Previous studies indicate that hAGP has 1 common drug binding site, which appears to be wide and flexible (61). Characterization of the binding site of UCN-01 on hAGP by Kurata *et al.* (58) revealed partial overlap with amino acid residues implicated in binding of basic drugs, acidic drugs, and steroid hormones. In a previous attempt to further characterize the binding site, we found that Trp-160 is particularly likely to play a major role in the binding of UCN-01. However, because that conclusion was the result of deducing the location of the 3 tryptophan residues, other experimental approaches are needed to confirm it. Currently, no x-ray crystallographic data is available for hAGP, which is a heterogeneous protein consisting of different isoforms and glycosylation states that hinder crystallization. Therefore, in the present study, we examined the possibility of using UCN-01 as a photoaffinity-labeling agent. An ideal photolabeling reagent is stable not only in storage but also under the conditions in which the experiments are performed. Another problem with reagent stability is covalent attachment in the dark, either specific or nonspecific, to the protein under study. All the advantages of photoaffinity labeling are lost if such covalent attachment occurs. In the present study, a covalent bond was formed between UCN-01 and hAGP only upon photoirradiation (Fig. 2).

The results of the present examination of photoinhibition by staurosporine and UCN-02 were as expected (Table I). It is interesting that a change in the configuration of the hydroxyl group of UCN-01 or substitution of a hydrogen atom at the C-7 position of UCN-01 caused a decrease in binding inhibition effects. This confirms our finding that the substituent at C-7 of the UCN-01 molecule governs the affinity of its binding to hAGP. On the other hand, the extensive photoinhibition by progesterone, but not warfarin or propranolol, suggests that the binding site of staurosporine analogs overlaps to a greater extent with the binding site of steroids. This sharing of a binding region between UCN-01 and steroids is thought to be of minimal clinical significance, given the increased hAGP concentration in cancer and the extremely high binding affinity of UCN-01 for hAGP.

Sequence analysis of the major radioactive tryptic peptides separated from hAGP photolabeled with [^{3}H]UCN-01 showed that these peptides correspond to amino acids Ser-153 to Lys-161 of hAGP. In addition, no phenylthiohydantoin (PTH) derivatives were detected at the 8th cycle, which corresponds to the 160th Trp residue (Fig. 7), indicating that the covalent bond formed upon photolabeling of [^{3}H]UCN-01 to hAGP is relatively stable under the conditions of Edman degradation, and that it is highly likely that Trp-160 was photolabeled by [^{3}H]UCN-01.

All naturally occurring genetic variants of hAGP conserve the 3 Trp residues in the protein amino acid sequence: Trp-25, Trp-122, and Trp-160 (64). It is noteworthy that there is no significant difference in the binding percentage of UCN-01 between the F1*S and A variants of hAGP (38). 2 of 3 Trp residues of hAGP are relatively shielded from the bulk solvent, whereas the third Trp residue is located on the periphery of the domain. It has been deduced that Trp-25 is located deep in the binding pocket, and that Trp-122 is located in the central hydrophobic pocket of the protein (65). This suggests that Trp-160 is the Trp residue that is exposed to the bulk solvent. We also used site-directed mutagenesis to identify the key Trp residue involved in UCN-01 binding. Photolabeling of wild-type and mutant rhAGP with [^{3}H]UCN-01 revealed that photoincorporation was significantly lower for W160A than for the wild type. In contrast, the level of photoincorporation observed for the other 2 mutants, W25A and W122A, was comparable to that of the wild type. These results strongly support the hypothesis that Trp-160 is the key amino acid responsible for the extraordinarily high affinity of binding between UCN-01 and hAGP.

Previous studies have revealed the structures of UCN-01 and staurosporine bound to the active conformations of Chk1 (47), phospho-CDK2/cyclin A (66), and PDK1 (67). Coincidentally, as observed in the present study, the most important differences previously observed between staurosporine and UCN-01 complexes are the contacts involving the 7-OH group of UCN-01. Komander *et al.* (67) analyzed the relative affinities of staurosporine and UCN-01 for 29 different kinases, and found that binding that was potently inhibited by UCN-01 tended to involve molecules with a side chain that can directly form a hydrogen bond with the 7-OH group of UCN-01. Taking into account the experimental spectra and the unfavorable docking energy, Zsila *et al.* (68) suggested that it is unlikely that curcumin binds inside the central cavity of hAGP. The present docking models show that UCN-01 can interact with surface clefts of hAGP containing Trp-160. The interacting amino acid residues identified by the present type II model are consistent with results of our previous experimental studies of chemical modifications and protein binding (38), as well as those of

present studies using photoaffinity labeling and site-directed mutagenesis.

In order to further analyze the binding cleft of type II docking model, staurosporine and UCN-02, a stereoisomer of UCN-01 with an α-OH group at the C-7 position, were used to replace UCN-01 at the same position to produce another two docking models (data not shown). In general, all interacting amino acid residues in the two latter models were similar to those of the former, except that the α-OH group at the C-7 position of UCN-02 interacts with COOH group of Glu-132, in contrast to UCN-01 where the C-7 β-OH group interacts with Lys-161. On the other hand, no interaction of any form with the amino acid side chain could be observed for the substituent at C-7 position of staurosporine where hydrogen atom exists. Another amino acid residue that deserved attention was Lys-135 as its distance from the sugar ring of UCN-02 was more than 5 Å, the greatest among the three models.

The following sequence of binding affinity for hAGP has previously been observed: UCN-01 > staurosporine > UCN-02 (38). The aromatic ring of UCN-01 is stacked on Trp-160, and the hydrophobic interaction is strengthened by the electrostatic interaction between the 7-OH group of UCN-01 and Lys-161, which are located on the same side of Trp-160. In contrast, the hydrogen bond between the 7-OH group of UCN-02 and Glu-132, which is located on the opposite side, appears to weaken the hydrophobic interaction, because the ring of UCN-02 has been diverted away from Trp-160. The aromatic ring of staurosporine is not diverted from Trp-160, due to the absence of the 7-OH group. In order to gain deeper insight on the binding mechanism of UCN-01 to hAGP, experiments using Glu-132 and Lys-161 hAGP mutants to examine the role of each mutated amino acid residue in the high affinity binding of UCN-01 is currently underway in our laboratory.

Staurosporine is a natural product derived from fermentation extracts of several bacterial species. Staurosporine was initially identified as a potent inhibitor of PKC, which is a Ca^{2+}- and phospholipid-activated kinase (69). Different isoforms of PKC are activated in response to growth factors that act on receptor tyrosine kinases and 7-transmembrane domain receptors (70). Studies have revealed that staurosporine is a broad-acting kinase inhibitor with little specificity or selectivity for PKC (71). Recently, the staurosporine analog *N*-benzoylstaurosporine (PKC412) has been reported to exhibit strong hAGP binding, and to have unusual pharmacokinetics similar to those of staurosporine, which were not predicted by animal studies (72). PKC412 is the only staurosporine inhibitor of protein kinases other than UCN-01 that has been subjected to a clinical trial. There has been a study of oral administration of PKC412 once daily (73). It is interesting that PKC412 exhibits complex pharmacology resulting from binding to hAGP. Preclinical experiments had shown extensive binding of PKC412 to human plasma proteins, with ~88–98% protein binding, depending on the drug concentration (72). Rates of binding of PKC412 to hAGP were particularly interesting. In the preclinical experiments, the plasma concentrations of PKC412 were higher, and the half-life was longer than predicted from animal studies and single dose kinetics studies with healthy volunteers (72). In contrast to UCN-01, PKC412 was metabolized to 7-hydroxy-PKC412 and an *O*-demethyl-PKC412, both of which also bound to hAGP. The major metabolite had a particularly long half-life (74). It is possible that PKC412 and its metabolite preferentially bind to hAGP *in vivo*, and this may account for the longer than anticipated plasma half-life. The dynamics of dissociation of PKC412 from plasma proteins and tissue distribution of PKC412 are likely to be complex, and plasma levels may not accurately reflect drug concentration in target tissues. Because plasma pharmacokinetic evaluation is complicated by protein binding and metabolism, studies using biologic markers of PKC inhibition can contribute to optimization of PKC412 administration.

CONCLUSIONS

Because of the potential implications of species-specific binding of UCN-01 to hAGP in human plasma for the development of staurosporine analogs, studies of analogs of UCN-01 and of PKC412, which lack hAGP binding or very weakly bind to hAGP, should be conducted along with studies of the potential usefulness of staurosporine pharmacophores. Characterization of the binding site of UCN-01 on hAGP using photoaffinity labeling and site-directed mutagenesis techniques has provided direct evidence that strongly indicates that Trp-160 plays an important role in the binding interaction between UCN-01 and hAGP. In addition to the obvious pharmacokinetic implications of the extraordinarily high affinity of binding of UCN-01 to hAGP, the present results suggest that hAGP is a suitable platform for further design of novel staurosporine analog anticancer drugs, and also for evaluation of side effects and drug interaction in clinical settings. The present results provide clues to the design of future second-generation therapeutic agents, and can serve as a basis for future studies of UCN-01 administered alone and in combination with other anticancer drugs, particularly DNA-damaging agents.

Acknowledgment—We thank Dr. Vladimir Kopecky, Jr. of the Institute of Physics, Charles University in Prague, for providing us with the protein moiety of hAGP in the native state and with docked progesterone in a PDB format.

REFERENCES

1. Schmid, K., Nimerg, R. B., Kimura, A., Yamaguchi, H., and Binette, J. P. (1977) *Biochim. Biophys. Acta* **492,** 291–302
2. Kremer, J. M., Wilting, J., and Janssen, L. H. (1988) *Pharmacol. Rev.* **40,** 1–47
3. Van Dijk, W. (1995) *Adv. Exp. Med. Biol.* **376,** 223–229
4. Hochepied, T., Berger, F. G., Baumann, H., and Libert, C. (2003) *Cytokine Growth Factor Rev.* **14,** 25–34
5. Cheresh, D. A., Haynes, D. H., and Distasio, J. A. (1984) *Immunology* **51,** 541–548
6. Morita, K., and Yamaji, A. (1995) *Ther. Drug Monit.* **17,** 107–112
7. Mackiewicz, A., and Mackiewicz, K. (1995) *Glycoconj. J.* **12,** 241–247
8. Duche, J. C., Urien, S., Simon, N., Malaurie, E., Monnet, I., and Barre, J. (2000) *Clin. Biochem.* **33,** 197–202
9. Fan, C., Stendahl, U., Stjernberg, N., and Beckman, L. (1995) *Oncology* **52,** 498–500
10. Mazoit, J. X., and Dalens, B. J. (2004) *Clin. Pharmacokinet.* **43,** 17–32
11. Veering, B. T., Burm, A. G., Feyen, H. M., Olieman, W. M., Souverijn, J. H., and Van Kleef, J. W. (2002) *Anesthesiology* **96,** 1062–1069
12. Hedaya, M. A., and Daoud, S. S. (2001) *Anticancer Res.* **21,** 4005–4010
13. Gambacorti-Passerini, C., Zucchetti, M., Russo, D., Frapolli, R., Verga, M., Bungaro, S., Tornaghi, L., Rossi, F., Pioltelli, P., Pogliani, E., Alberti, D., Corneo, G., and D'Incalci, M. (2003) *Clin. Cancer Res.* **9,** 625–632
14. Bruno, R., Olivares, R., Berille, J., Chaikin, P., Vivier, N., Hammershaimb, L., Rhodes, G. R., and Rigas, J. R. (2003) *Clin. Cancer Res.* **9,** 1077–1082
15. Takahashi, I., Kobayashi, E., Asano, K., Yoshida, M., and Nakano, H. (1987) *J. Antibiot (Tokyo)* **40,** 1782–1784
16. Penuelas, S., Alemany, C., Noe, V., and Ciudad, C. J. (2003) *Eur. J. Biochem.* **270,** 4809–4822
17. Yu, Q., La, Rose, J., Zhang, H., Takemura, H., Kohn, K. W., and Pommier, Y. (2002) *Cancer Res.* **62,** 5743–5748
18. Facchinetti, M. M., De, Siervi, A., Toskos, D., and Senderowicz, A. M. (2004) *Cancer Res.* **64,** 3629–3637
19. Dai, Y., Pei, X. Y., Rahmani, M., Conrad, D. H., Dent, P., and Grant, S. (2004) *Blood* **103,** 2761–2770
20. Tenzer, A., and Pruschy, M. (2003) *Curr. Med. Chem. Anti-Cancer Agents* **3,** 35–46
21. Akinaga, S., Gomi, K., Morimoto, M., Tamaoki, T., and Okabe, M. (1991) *Cancer Res.* **51,** 4888–4892
22. Akinaga, S., Nomura, K., Gomi, K., and Okabe, M. (1994) *Cancer Chemother. Pharmacol.* **33,** 273–280
23. Seynaeve, C. M., Stetler-Stevenson, M., Sebers, S., Kaur, G., Sausville, E. A., and Worland, P. J. (1993) *Cancer Res.* **53,** 2081–2086
24. Senderowicz, A. M. (2003) *Oncogene* **22,** 6609–6620
25. Akiyama, T., Yoshida, T., Tsujita, T., Shimizu, M., Mizukami, T., Okabe, M., and Akinaga, S. (1997) *Cancer Res.* **57,** 1495–1501
26. Akinaga, S., Nomura, K., Gomi, K., and Okabe, M. (1993) *Cancer Chemother. Pharmacol.* **32,** 183–189
27. Abe, S., Kubota, T., Otani, Y., Furukawa, T., Watanabe, M., Kumai, K., and Kitajima, M. (2000) *Jpn. J. Cancer Res.* **91,** 1192–1198
28. Bunch, R. T., and Eastman, A. (1996) *Clin. Cancer Res.* **2,** 791–797